

experiments: "Reduction" refers to methods that enable researchers to obtain comparable levels of information from fewer animals or to obtain more information from the same number of animals; "Refinement" refers to methods that alleviate or minimize potential pain, suffering or distress, and enhance the welfare of the animals used; and "Replacement" refers to the preferred use of non-animal methods over animal methods whenever it is possible to achieve the same scientific aims.

We therefore used silicone membrane as an alternative to skin membrane to determine the skin concentration of cosmetic ingredients or drugs, from the viewpoints of the great necessity of estimating their concentration in the skin in the development of cosmetics or topical formulations, and as an animal experiment alternative. Silicone membrane has been used as an alternative to skin membrane, and the permeation of cosmetic ingredients and drugs through the silicone membranes was compared with that through human or animal skin (8–11). Few experiments have been performed, however, on their skin or membrane concentration. In the present study, a method for estimating skin concentration was established using silicone membrane permeability. A series of parabens (methyl, ethyl, *n*-propyl, *n*-butyl esters) were used as model penetrants, since they have very different lipophilicities (*i.e.*, *n*-octanol/water partition coefficient) in spite of having a similar molecular weight (152–194 Da). Table I summarizes the physicochemical properties of parabens used in this experiment (12).

THEORETICAL (13,14)

One-Layered Diffusion Model (15)

Determination of Membrane Concentration

The diffusion of chemical compounds in the membrane is expressed theoretically by Fick's second law of diffusion, $\frac{\partial C}{\partial t} = D \frac{\partial^2 C}{\partial x^2}$, under the assumption that the membrane is a homogeneous single layer, where C is the penetrant concentration in the membrane at position, x , and time, t . When a sink condition is assumed on the receiver side of the membrane, *i.e.*, $x = L$, a set of initial conditions ($C=0$ at $t=0$ and $0 < x < L$) and boundary conditions ($C = KC_v$ at $x=0$ and $C=0$ at $x=L$, where K is the partition coefficient of the penetrant from the vehicle to membrane and C_v is the penetrant concentration in the vehicle) are obtained (see Fig. 1a).

Then, membrane concentration, C , and its steady-state level at an infinite time, C_{ss} , are expressed as follows (12):

$$C = KC_v \left\{ \left(1 - \frac{x}{L} \right) - \frac{2}{\pi^2} \sum_{n=1}^{\infty} \sin \frac{n\pi x}{L} \exp \left(-\frac{Dn^2\pi^2 t}{L^2} \right) \right\} \quad (1)$$

$$C_{ss} = KC_v \left(1 - \frac{x}{L} \right) \quad (2)$$

Further, the mean membrane concentrations of penetrant, \bar{C} and \bar{C}_{ss} , are obtained by integrating C in Eqs. 1 and 2 from $x=0$ to L :

$$\bar{C} = \frac{KC_v}{2} \left\{ 1 - \frac{8}{\pi^2} \sum_{m=1}^{\infty} \frac{1}{(2m-1)^2} \exp \left(-\frac{D(2m-1)^2\pi^2 t}{L^2} \right) \right\} \quad (3)$$

$$\bar{C}_{ss} = \frac{KC_v}{2} \quad (4)$$

As shown in Eq. 4, the mean membrane concentration of the penetrant can be determined by K and C_v , not by D . Because C_v is a known parameter, a parameter, K , is the only determinant of the mean membrane concentration of the penetrant.

Determination of Membrane Permeation

Since the silicone membrane can be supposed to be homogenous in one layer, the permeation profiles of parabens throughout the membrane were analyzed using a one-layered diffusion model (16,17). Under the initial and boundary conditions shown above, the amount of drug permeating the unit area of the silicone membrane at time t , Q , can be represented as

$$Q = KLC_v \left[\frac{D}{L^2} t - \frac{1}{6} - \frac{2}{\pi^2} \sum_{n=1}^{\infty} \frac{(-1)^n}{n^2} \exp \left(-\frac{D}{L^2} n^2 \pi^2 t \right) \right] \quad (5)$$

The partition parameter ($K \cdot L$) and diffusion parameter (D/L^2) were obtained by curve fitting the obtained data to Eq. 5 using the least squares method. In the calculation of D and K , the thickness of the silicone membrane was fixed at 68 μm . Permeability coefficient, P , was calculated by an equation, $P = \frac{KD}{L}$.

Table I. Physicochemical Parameters of Parabens

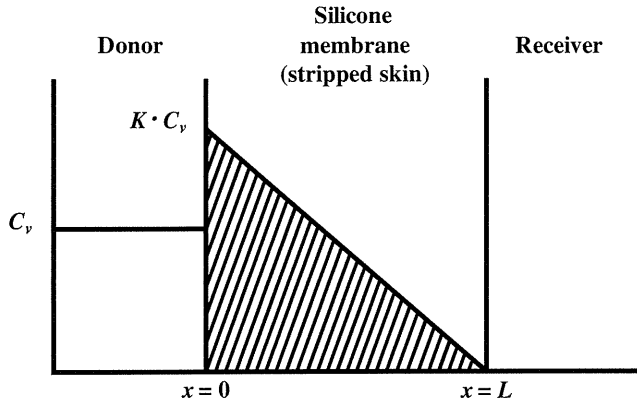
	Methyl paraben (MP)	Ethyl paraben (EP)	Propyl paraben (PP)	Butyl paraben (BP)
<i>M.W.</i>	152.12	166.18	180.20	194.23
<i>Log K_{ow}</i> ^{a)}	0.940	1.93	2.27	3.53
<i>clog P</i> ^{b)}	1.98	2.51	3.04	3.57
Solubility ^{c)} (mM)	19.7	8.82	2.27	1.60

^{a)} *n*-Octanol / water partition coefficient at 37°C

^{b)} Calculation by software, Chem Draw (CambridgeSoft)

^{c)} In water at 32°C

a One-layered diffusion model



b Two-layered diffusion model

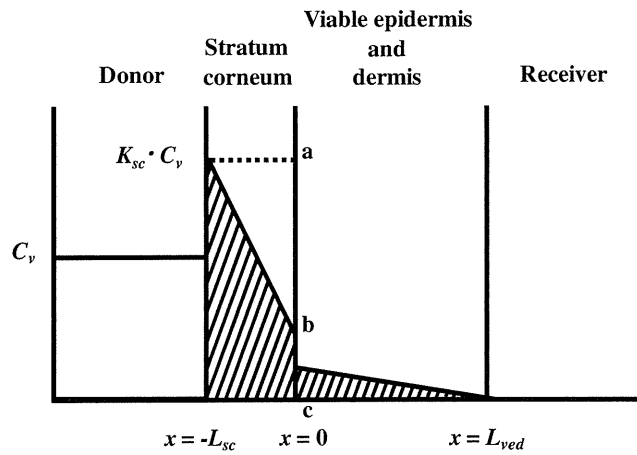


Fig. 1. Schematic diagram of concentration-distance profile in one- and two-layered diffusion membrane models in membrane permeation experiments. Membrane thickness is L and $L_{sc} + L_{ved}$ for one- and two-layered diffusion membranes models, respectively. C_v is the donor concentration of parabens, and K and K_{sc} are partition coefficients to membranes.

Stripped hairless rat skin was treated as a homogeneous layer, the same as the silicone membrane.

Two-Layered Diffusion Model

Determination of Membrane Concentration Using Two-Layered Diffusion Model

Fig. 1b shows a typical two-layered diffusion model of skin. Penetrant concentration in the first layer of skin, the stratum corneum, C_{sc} , and that in the second layer, the viable epidermis and dermis of skin, C_{ved} , can be expressed by Fick's second law of diffusion. Similarly, initial conditions and boundary conditions are represented. Boundary condition between the first and second layer is $C_{ved} = K_{sc}K_{ved}C_{sc}$ and $D_{sc} \frac{dC_{sc}}{dx} = D_{ved} \frac{dC_{ved}}{dx}$, where K_{sc} and K_{ved} are partition coefficients of the penetrant from the vehicle to stratum corneum and to the viable epidermis and dermis, and D_{sc} and D_{ved} are diffusion coefficients in the stratum corneum and viable epidermis and dermis, respectively.

In the two-layered diffusion model, the overall permeability coefficient, P_{tot} , can be expressed by that in the

stratum corneum, P_{sc} , and in the viable epidermis and dermis, P_{ved} , as follows, in Eq. 6. (18):

$$\frac{1}{P_{tot}} = \frac{1}{P_{sc}} + \frac{1}{P_{ved}} \quad (6)$$

In addition, the reciprocal of the permeability coefficient can be replaced with permeation resistant, R , and the following equation can be derived, as Eq. 7:

$$R_{tot} = R_{sc} + R_{ved} \quad (7)$$

The permeation resistance of the penetrants can be represented as in the electric circuit. Two resistances, R_{sc} and R_{ved} , exist in the skin membrane, as shown in Fig. 1b. The ratio of the Line segment ab against bc at the surface between the stratum corneum and viable epidermis, $x=0$, should be the ratio of R_{sc} against R_{ved} . Thus, the penetrant concentration at point b, C_b , can be represented by

$$C_b = K_{sc}C_v \frac{R_{ved}}{R_{tot}} \quad (8)$$

The amount of penetrant in the unit area of the stratum corneum, M_{sc} , can be represented using Eq. 8 as Eq. 9.

$$M_{sc} = \frac{K_{sc}C_vL_{sc} \left(1 + \frac{R_{ved}}{R_{tot}}\right)}{2} \quad (9)$$

Since the partition coefficient of the penetrant from the stratum corneum to the viable epidermis and dermis is represented as K_{ved}/K_{sc} , the amount of penetrant in the unit area of the viable epidermis and dermis, M_{ved} , can be represented as

$$M_{ved} = \frac{K_{ved}C_vL_{ved} \frac{R_{ved}}{R_{tot}}}{2} \quad (10)$$

By summation of Eqs. 9 and 10, M_{tot} , the drug amount in the unit area of the skin can be represented as follows:

$$M_{tot} = \frac{C_v}{2} \left\{ K_{sc}L_{sc} \left(1 + \frac{R_{ved}}{R_{tot}}\right) + K_{ved}L_{ved} \frac{R_{ved}}{R_{tot}} \right\} \quad (11)$$

By dividing M_{tot} in Eq. 11 by skin thickness, L_{tot} , the average drug concentration in the skin, \bar{C}_{ss} , is

$$\bar{C}_{ss} = \frac{C_v}{2L_{tot}} \left\{ K_{sc}L_{sc} \left(1 + \frac{R_{ved}}{R_{tot}}\right) + K_{ved}L_{ved} \frac{R_{ved}}{R_{tot}} \right\} \quad (12)$$

When resistances, R , are changed to permeability coefficients, P , finally Eq. 13 is derived,

$$\bar{C}_{ss} = \frac{C_v}{2L_{tot}} \left\{ K_{sc}L_{sc} \left(1 + \frac{P_{tot}}{P_{ved}}\right) + K_{ved}L_{ved} \frac{P_{tot}}{P_{ved}} \right\} \quad (13)$$

Determination of Membrane Permeation Using Two-Layered Diffusion Model

Two diffusion coefficients, D_{sc} and D_{ved} , and two partition coefficients, K_{sc} and K_{ved} , were obtained by curve fitting the cumulative amount of parabens that permeated through the full-thickness skin and stripped skin to the

theoretical values using the least squares method, where theoretical values were expressed by two diffusion equations (Fick's second law) showing the diffusion profiles in the stratum corneum and viable epidermis and dermis. Differential equations describing Fick's second law are as follows (14):

$$\frac{dC_{ij}}{dt} = \frac{1}{\Delta t} (C_{ij+1} - C_{ij}) \quad (14)$$

$$\frac{d^2C_{ij}}{dx^2} = \frac{1}{\Delta x^2} (C_{i-1j} - 2C_{ij} + C_{i+1j}) \quad (15)$$

Mathematical treatment for determining the skin permeation using two-layered diffusion model was the same as in our previous method (14).

Calculation of Permeation Parameters

Generally, most resistance against drug permeation throughout hairless rat skin is in the stratum corneum (17). Rat skin was also treated as a single-layered membrane, the same as the silicone membrane. Parameters D and K were calculated under the assumption that the stratum corneum is a homogeneous membrane with a thickness of 15 μm .

Calculation of Theoretical Membrane Concentration of Parabens

The theoretical membrane concentration of parabens was calculated by Eq. 6 and the K value obtained from the membrane permeation study.

EXPERIMENT

Reagents and Materials

Parabens: methyl paraben (MP), ethyl paraben (EP), *n*-propyl paraben (PP), and *n*-butyl paraben (BP) were obtained from Tokyo Kasei Chemical Co., Ltd. (Tokyo, Japan). An esterase inhibitor, diisopropyl fluorophosphate (DFP), and a deproteinization agent, trichloroacetic acid (TCA), were obtained from Wako Pure Chemical Industries, Ltd. (Osaka, Japan). Other reagents and solvents were liquid chromatograph and special grade chemicals.

The silicone membrane (Dow Corning 7-4107) was a gift from Nagase & Co., Ltd. (Tokyo, Japan).

Experimental Animals

Male hairless rats (WBM/ILA-Ht, 230–280 g) were obtained from the Life Science Research Center, Josai University (Sakado, Saitama, Japan) or Ishikawa Experimental Animal Laboratories (Fukaya, Saitama, Japan). All animal experiments were performed according to the ethics committee of Josai University.

Membrane Permeation Experiments of Parabens

The silicone membrane was set on a Franz-type diffusion cell (receiver cell volume: 6.0 mL, effective diffusion area: 1.77 cm^2) using cyanoacrylate glue (19–22). Phosphate-buffered saline (pH 7.4, PBS) was applied to the receiver cell and maintained at 32°C

for 15 min. Aliquots (0.5 mL) of different concentrations of parabens (MP 10 mM, EP 5 mM, PP 1 mM, BP 0.5 mM) in PBS were applied to the donor cell to start the permeation experiment. The experimental setup is shown in Fig. 2. The receiver solution was stirred on a magnetic stirrer with a bar; the experiment was performed at 32°C. At predetermined intervals, 400 μL of the receiver solution was sampled, and the same volume of PBS was added to the receiver cell to keep the volume constant. Paraben concentration was determined by HPLC.

Abdominal skin (full-thickness skin or stripped skin) was excised from hairless rats under pentobarbital (25 mg/kg, *i.p.*) anesthesia, and debris and excess fat were trimmed off the excised skin. Stripped skin was made by tape-stripping the stratum corneum 20 times before excising from rats (23). The obtained skin piece was then set on the Franz-type diffusion cell, as above. DFP (2.7 $\mu\text{mol/mL}$ in PBS) was applied to the receiver cell for half an hour (12,24–26). After rinsing off the reagent, paraben solution (0.5 mL) in PBS and DFP in PBS (0.54 $\mu\text{mol/mL}$, 6.0 mL) were added to the donor and receiver cells, respectively, to start the skin permeation experiment. Other procedures were consistent with the silicone membrane permeation experiments.

Determination of Extraction Ratio of Parabens

Silicone Membrane. Silicone membrane was loaded with parabens in chloroform and dried. Fresh chloroform (1 mL) was then applied to the silicone membrane piece. After agitating for 15 min, the resulting chloroform was sampled, and fresh chloroform was again added for the second extraction of parabens. Total chloroform containing parabens was evaporated to dryness, and the sample was reconstituted with 1.0 mL acetonitrile. The sample was injected onto HPLC to determine the paraben concentration. The extraction ratio of parabens from silicone membrane was almost 1.0.

Hairless Rat Skin. Hairless rat skin was loaded with parabens in water, and the skin piece was minced with scissors and homogenized at 12,000 rpm using a homogenizer (Polytron PT-MR 3000; Kinematica Inc., Littau, Switzerland) for 5 min at 4°C. The homogenate was incubated for 1 h at 32°C. The same volume of 16% TCA was added to the skin homogenate and agitated for 15 min (27–29). The supernatant after centrifugation (15,000 rpm, 5 min, 4°C) was injected onto HPLC. Parabens were extracted from the skin homogenate using chloroform, as in the silicone membrane experiment. The extraction ratio of parabens was almost 1.0.

Determination of Paraben Concentration in Silicone Membrane and Hairless Rat Skin

Silicone Membrane. After the permeation experiment, the donor solution was removed, and the silicone membrane was washed with PBS (1 mL). Chloroform (1 mL) was added to the silicone membrane in the Franz-type diffusion cell (permeation area: 1.77 cm^2) and agitated for 15 min to extract parabens from the membrane. The subsequent procedure was consistent with Determination of Extraction Ratio of Parabens.

Hairless Rat Skin. After the permeation experiment, the donor solution was removed, and the stratum corneum side

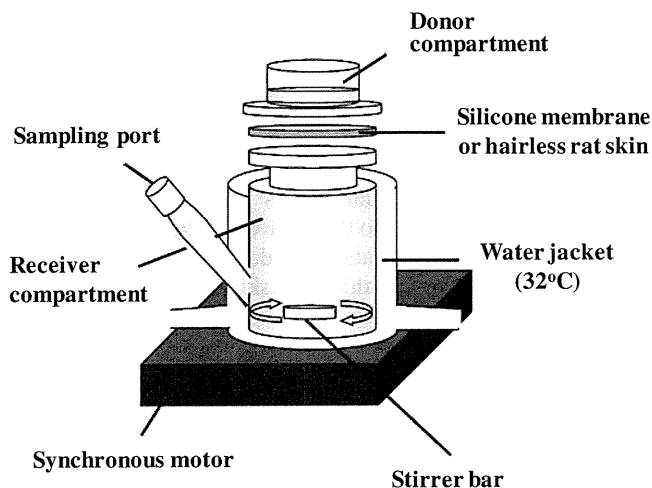


Fig. 2. Schematic representation of permeation experiment using silicone membrane and hairless rat skin.

of hairless rat skin was washed two times with PBS (1 mL). The rat skin was taken from the diffusion cell, and the permeation area of the skin (1.77 cm^2) was kept in a freezer (-15°C) before determining the skin concentration. This frozen skin was minced with scissors, and PBS (1 mL) was added to homogenize the minced skin (12,000 rpm, 5 min, 4°C). The subsequent procedure was consistent with Determination of Extraction Ratio of Parabens.

Determination Methods of Parabens

The same volume of acetonitrile containing an internal standard (another paraben) was added to the paraben samples. After slight mixing, the sample was injected onto HPLC. The HPLC system consists of a pump (LC-10 AD; Shimadzu, Kyoto, Japan), Chromatopac (C-R6A; Shimadzu), UV detector (SPD-6A; Shimadzu), system controller (SCL-6B; Shimadzu) and an auto-injector (SIL-7A; Shimadzu). The column was LiChroCART®250-4 (KGaA-64271; Merck, Darmstadt, Germany) kept at 40°C during the eluting mobile phase, 0.1% phosphoric acid : acetonitrile = 75 : 25 for MP and EP and 0.1% phosphoric acid : acetonitrile = 55 : 45 for PP and BP. The flow rate was 1.0 mL/min. The injection volume was $20 \mu\text{L}$, and detection was performed at 260 nm.

RESULTS AND DISCUSSIONS

Partition Coefficient and Concentration of Parabens into and in the Silicone Membrane

Since drug distribution in the skin membrane is a physical phenomenon, it can be evaluated using artificial membranes as well as human and animal skin. A silicone membrane was used in this experiment due to its cost and easy availability.

The direct measurement of drug concentration in the membrane has several problems. Generally, only one data point is obtained from one membrane after drug application. In addition, controlling the removal of the drug formulation from the membrane surface is very difficult. Hard cleaning of

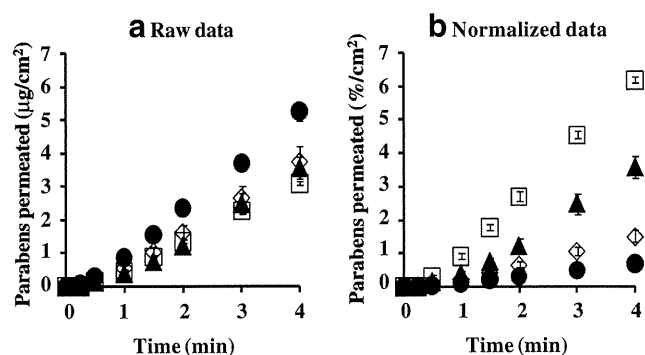


Fig. 3. Time course of the cumulative amount of parabens that permeated the silicone membrane. (a) raw data, (b) normalized data. Symbols: ●: 10 mM MP, ○: 5 mM EP, ▲: 1 mM PP, □: 0.5 mM BP. Each data point represents the mean \pm S.E. ($n=4-8$).

the membrane surface decreases the membrane concentration, whereas inadequate cleaning may leave the drug formulation on the membrane. We first performed the membrane permeation experiment, and permeation parameters were obtained. The membrane concentration can be calculated using the partition coefficient, K , of the applied drug from the vehicle to the membrane, as shown in Eq. 6. Next, the calculated values were compared with the directly observed membrane concentration. The membrane was obtained after the membrane permeation experiments.

Fig. 3 shows the cumulative amount of parabens that permeated the silicone membrane. Fig. 3a and b show raw and normalized data (raw data divided by application concentration of parabens (19,30)), respectively. The permeation ratio of BP against the application amount was highest, followed by PP, EP and MP. The increase in the lipophilicity of parabens increased the permeability, as shown in Fig. 3b (31).

Generally, high permeability and solubility of chemicals through and in the membrane are observed when the solubility parameter of chemicals is close to that of membrane. The solubility parameter of BP, $10.9 \text{ (cal/cm}^3)^{1/2}$, is closest to that of the silicone membrane ($7.3-7.5 \text{ (cal/cm}^3)^{1/2}$) among the parabens (MP: $11.5 \text{ (cal/cm}^3)^{1/2}$, EP: $11.3 \text{ (cal/cm}^3)^{1/2}$, PP: $11.1 \text{ (cal/cm}^3)^{1/2}$) used in this experiment (32-34).

Fig. 4a and b show the observed concentration and normalized concentration corrected using the application concentration of parabens in the silicone membrane, respectively. Each concentration is that at the steady state after

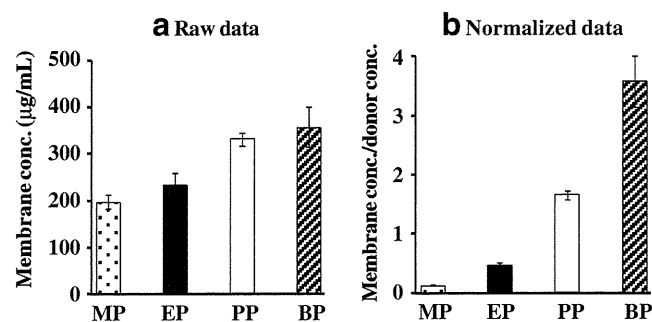


Fig. 4. Raw data (a) and normalized data [(silicone membrane concentration)/(donor concentration)] (b) for steady-state silicone membrane concentration of parabens. Each column represents the mean \pm S.E. ($n=4-8$).

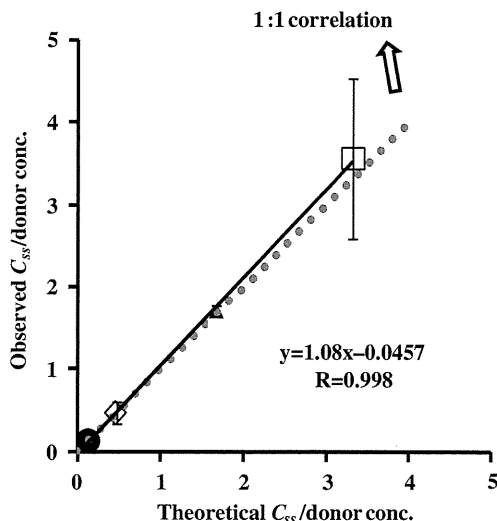


Fig. 5. Relationship between theoretical and observed steady-state silicone membrane concentration of parabens. Normalized data were used (see Fig. 4). One-layered diffusion membrane model was used to obtain theoretical steady-state membrane concentration of parabens. Symbols: see Fig. 3. The observed data represent the mean \pm S.D. ($n=4-8$). Almost 1:1 correlation was found. K , D and P were as follows ($D : \times 10^{-7} \text{ cm}^2/\text{s}$, $P : \times 10^{-5} \text{ cm/s}$): MP ($K=0.256$, $D=4.07$, $P=1.53$), EP ($K=0.907$, $D=2.60$, $P=3.47$), PP ($K=3.34$, $D=1.78$, $P=8.76$), and BP ($K=6.64$, $D=1.65$, $P=16.1$).

starting the permeation experiments. An increase in K_{ow} of parabens increases the membrane concentration.

Fig. 5 shows the relationship between the theoretical and observed values of paraben concentration in the silicone membrane. This figure shows almost a 1:1 relationship between them, suggesting that the silicone membrane can be assumed to be one homogenous layer and that the membrane concentration of parabens can be theoretically determined by C_v and K . These results also suggest that the permeation experiment is useful to determine the membrane concentration. The figure also contains the permeation parameters of parabens in the legend. The permeation parameters were obtained by curve-fitting the permeation profiles to Fick's law of diffusion using the nonlinear least squares method, under the assumption that the silicone membrane is one homogenous layer. The permeability coefficient, P , of MP and BP was lowest and highest among the parabens used in this experiment. The diffusion coefficient, D ,

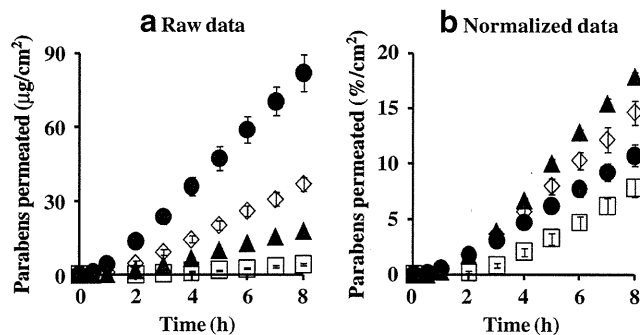


Fig. 6. Time course of the cumulative amount of parabens that permeated hairless rat intact skin. (a) raw data, (b) normalized data Symbols: see Fig. 3. Each data point represents the mean \pm S.E. ($n=5-11$).

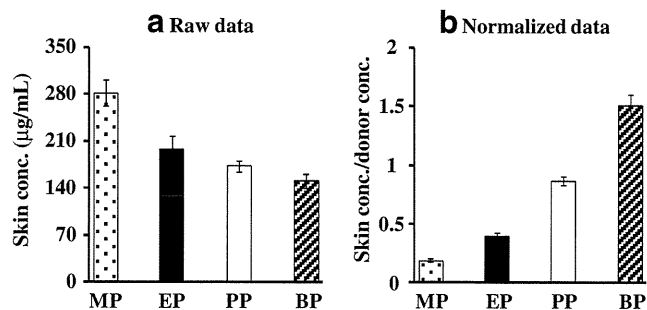


Fig. 7. Raw data (a) and normalized data [(skin concentration)/ (donor concentration)] for steady-state hairless rat skin concentration of parabens. Each column represents the mean \pm S.E. ($n=5-11$).

of these parabens in the silicone membranes was not so different (only 2-3 times different), whereas partition coefficient, K , was very different among these parabens (26 times different between MP and BP). A very different permeability coefficient, P , is closely related to the K of parabens. Since the P -value of parabens throughout the silicone membrane was very high (about 10^{-5} cm/s), the permeation profiles can be evaluated in a short experimental period. The theoretical membrane concentration of parabens calculated from the K -value was very close to the observed membrane concentration.

Membrane Permeation and Concentration: Comparison Between Silicone Membrane and Animal Skin

The theoretical concentration of parabens in silicone membrane, which was calculated from partition coefficient, K , was close to the observed concentration. A similar trial was carried out for the paraben concentration in hairless rat skin. Partition and skin concentration of parabens in rat skin were compared to those in the silicone membrane.

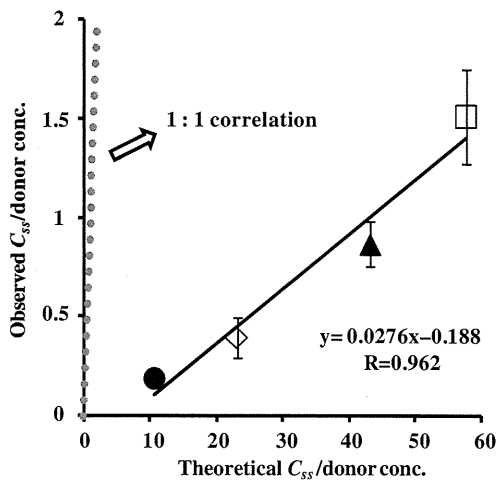


Fig. 8. Relationship between theoretical and observed steady-state hairless rat skin concentration of parabens. Normalized data were used (see Fig. 7). One-layered diffusion membrane model was used to obtain theoretical steady-state membrane concentration of parabens. Symbols: see Fig. 3. The observed data represent the mean \pm S.D. ($n=5-11$). The obtained line was very different from 1:1 correlation. K , D and P were as follows ($D : \times 10^{-11} \text{ cm}^2/\text{s}$, $P : \times 10^{-6} \text{ cm/s}$): MP ($K=21.3$, $D=14.2$, $P=2.03$), EP ($K=46.1$, $D=10.2$, $P=3.15$), PP ($K=86.3$, $D=6.67$, $P=3.84$), and BP ($K=115$, $D=1.63$, $P=1.26$).

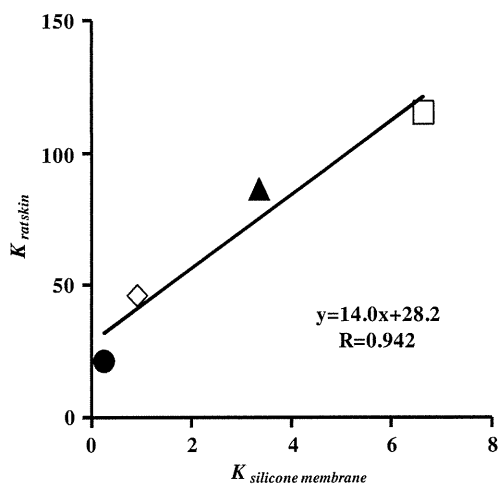


Fig. 9. Relationship between K to silicone membrane and K to rat skin (one-layered diffusion model). Symbols: see Fig. 3. Each data point represents the mean \pm S.E. ($n=4-8$ in silicone membrane data and 5-11 in rat skin data).

Fig. 6 shows the cumulative amount of parabens that permeated the excised hairless rat skin. Fig. 6a and b show the mean raw data and normalized permeation data. The latter was normalized by the application amount of parabens. The raw skin permeation data of parabens, as shown in Fig. 6a, are similar to silicone membrane permeation; however, the permeability coefficient ratio of BP against MP in hairless rat skin was much larger than that in the silicone membrane. This may have been due to the different permeation pathways between the silicone membrane and rat skin. The silicone membrane is a homogeneous membrane, whereas hairless rat skin has appendages, such as hair follicles, as well as the stratum corneum pathway. Interestingly, BP permeation through the silicone membrane was highest in the normalized data (Fig. 3b) among the parabens used in the present study, whereas PP permeation through rat skin was highest (Fig. 6b). These data are probably due to similar solubility parameter of BP or PP to that of the silicone membrane or rat skin, respectively.

Fig. 7a and b show the observed and normalized concentrations of parabens corrected using their application concentrations in hairless rat skin, respectively. Each paraben concentration in rat skin was that at the steady state after

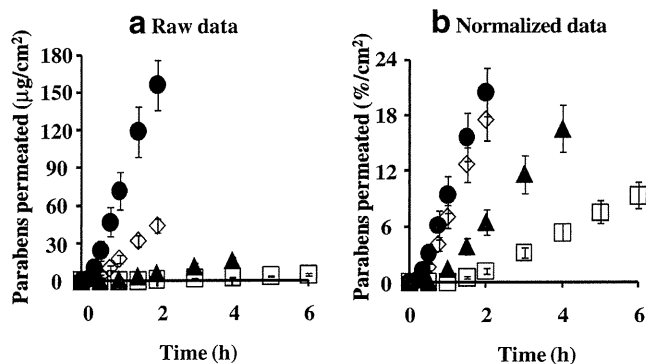


Fig. 10. Time course of the cumulative amount of parabens that permeated hairless rat stripped skin. (a) raw data, (b) normalized data. Symbols: see Fig. 3. Each data point represents the mean \pm S.E. ($n=3$).

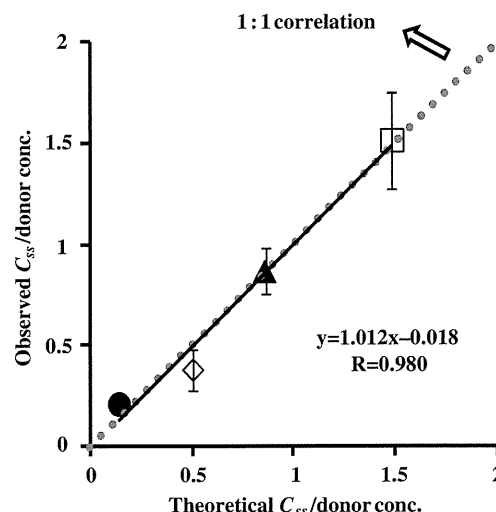


Fig. 11. Relationship between theoretical and observed C_{ss} in hairless rat skin. Normalized data were used (see Fig. 7). Two-layered diffusion membrane model was used to obtain theoretical steady-state skin concentration of parabens. Symbols: see Fig. 3. The observed data represent the mean \pm S.D. ($n=3-8$). Almost 1:1 correlation was found. K , D and P were as follows ($D_{sc} : \times 10^{-10}$ cm²/s, $P_{tot} : \times 10^{-6}$ cm/s, $D_{ved} : \times 10^{-7}$ cm²/s, $P_{ved} : \times 10^{-5}$ cm/s): MP ($K_{sc}=4.55$, $D_{sc}=9.38$, $P_{tot}=2.46$, $K_{ved}=2.95$, $D_{ved}=3.66$, $P_{ved}=1.85$), EP ($K_{sc}=9.18$, $D_{sc}=9.36$, $P_{tot}=5.73$, $K_{ved}=5.23$, $D_{ved}=2.19$, $P_{ved}=1.96$), PP ($K_{sc}=48.6$, $D_{sc}=5.72$, $P_{tot}=0.859$, $K_{ved}=2.57$, $D_{ved}=1.78$, $P_{ved}=0.628$), and BP ($K_{sc}=42.3$, $D_{sc}=9.73$, $P_{tot}=1.25$, $K_{ved}=4.58$, $D_{ved}=0.325$, $P_{ved}=0.348$).

starting the skin permeation experiment. As in the silicone membrane, the increase in partition coefficient, K , of parabens increased the skin concentration. The increment, however, was marked in the silicone membrane concentration, not in rat skin, except MP. This is due to the similar solubility parameter of parabens to that in the silicone membrane.

Fig. 8 shows the relation between the theoretical and observed skin concentrations of parabens. Although no 1:1 relationship was observed, a linear relation was found. When skin permeation data of a series of compounds are obtained,

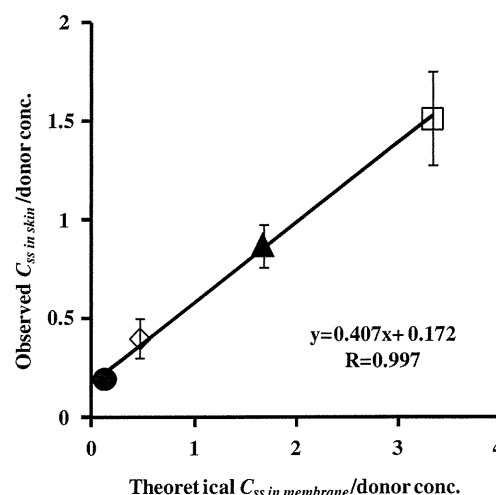


Fig. 12. Relationship between theoretical C_{ss} in silicone membrane/donor concentration and observed C_{ss} in rat skin/donor concentration. Symbols: see Fig. 3. Each data point represents the mean \pm S.D. ($n=3-8$).

the skin concentration of the compounds may be theoretically calculated. The figure also contains the obtained permeation parameters of parabens in the figure legend, under the assumption that the skin membrane is one homogenous layer. Compared to the silicone membrane, lower P and D and higher K were observed in the rat skin. Unfortunately, the theoretical skin concentration of parabens was much higher than the observed skin concentration. This lack of a 1:1 relationship is due to the assumption that the skin is one homogenous layer.

Fig. 9 illustrates the relationship between K and silicone membrane and rat skin (11). The two K values have a linear relation. These results suggest that the skin concentration of parabens cannot be easily predicted by calculating the skin permeation profiles because of the simple assumption about the skin membrane.

Simulation of Skin Concentration of Parabens

We then assumed that skin consists of two diffusion layers, of which the first layer is the stratum corneum and the second layer is the viable epidermis and dermis. The partition coefficient from the vehicle to the stratum corneum and that to the viable epidermis and dermis was obtained from permeation data through full-thickness and stripped skin.

First, the stripped-skin permeability of parabens was measured. Fig. 10a and b show raw and normalized permeation profiles through stripped skin. Tape stripping of the stratum corneum increased the skin permeation of parabens, especially hydrophilic parabens such as MP.

Fig. 11 shows the relation between the observed and calculated skin concentrations. The figure also summarizes the obtained permeation parameters of parabens in the legend. The theoretical values are close to the observed values, although little difference was found, which may be dependent on the process of washing the skin surface. The two-layered model predicts the skin concentration of parabens from skin permeation experiments much better than the one-layered model of hairless rat skin. Human and animal skins have appendages, such as hair follicles and sweat ducts, as additional permeation pathways to the primary permeation pathway, the stratum corneum (21). The hydrophilic pathway and the lipophilic pathway play a role in the overall skin permeation of several compounds. The contribution of appendages and the hydrophilic pathway must be taken into account to better predict the skin concentration of materials from skin permeation profiles.

Fig. 12 shows the relationship between the theoretical concentration of parabens in the silicone membrane and the normalized observed concentration of parabens in hairless rat skin. The very high correlation coefficient, 0.997, between them suggests the high predictability of the skin concentration of parabens using silicone membrane permeation experiments.

We supposed a homogenous one-layered model for the silicone membrane and two-layered model consisted of stratum corneum and the following layer for the rat skin. Although these membrane models were different, their concentration-distance profiles and theoretical concentrations of drug or cosmetic ingredient in both the membranes can be expressed only by physical diffusion model. Thus, membrane concentration in the two-layered diffusion model can be

easily replaced by that in the one-layered model using a mathematical approach. This is a reason why diffusion profile through silicone membrane is useful to predict the skin concentration of drugs or cosmetic ingredients.

In the near future, we plan to use broad compounds other than parabens, which are a simple series of compounds. We also plan to use several topical formulations, such as creams, ointments and patches. A silicone membrane permeation study using broad compounds from several formulations will produce a monogram of how to estimate the skin concentration of materials. All topical drugs have different target sites in skin tissues. Distribution of the skin concentration must be clarified from the shallow to deep layer in the near future. Since this is an alternative method to human and animal studies, it can be easily used by pharmaceutical and cosmetic companies to estimate the skin concentration after applying topical drug formulations and cosmetics.

CONCLUSION

The drug concentration in the silicone membrane and animal or human skin can be easily predicted using diffusion equations and membrane permeation data. This method can be applied to the design of cosmetic and topical pharmaceutical formulations. A silicone membrane can be used as an alternative membrane to human and animal skin.

ACKNOWLEDGEMENT

The authors are grateful to Mr. Yosuke Urabe and Mr. Masayasu Sugiura, Nagase & Co., Ltd. (Tokyo, Japan) for information on the silicone membrane.

REFERENCES

1. Knepp VM, Hadgraft J, Guy RH. Transdermal drug delivery: Problems and possibilities. *Critical Rev Ther Drug Carrier Sys.* 1987;4:13–37.
2. Singh P, Roberts MS. Iontophoretic transdermal delivery of salicylic acid and lidocaine to local subcutaneous structures. *J Pharm Sci.* 1993;82:127–31.
3. McNeill SC, Potts RO, Francoeur ML. Local enhanced topical delivery (LETD) of drugs: Does it truly exist? *Pharm Res.* 1992;9:1422–7.
4. Lodén M, Ungerth L, Serup J. Changes in European legislation make it timely to introduce a transparent market surveillance system for cosmetics. *Acta Dermato-Venereol.* 2007;87:485–92.
5. Toyoda H. Regulation of the animal experiments and testing in EU. *Envir Mutagen Res.* 2005;27:125–8.
6. Kolar R. Animal experimentation. *Sci Eng Ethics.* 2006;12:111–22.
7. Spielmann H. Animal use in the safety evaluation of chemicals: harmonization and emerging needs. *ILAR J.* 2002;43(Suppl):S11–7.
8. Leveque N, Raghavan SL, Lane ME, Hadgraft J. Use of a molecular form technique for the penetration of supersaturated solutions of salicylic acid across silicone membranes and human skin *in vitro*. *Int J Pharm.* 2006;318:49–54.
9. Ottaviani G, Martel S, Carrupt P. Parallel artificial membrane permeability assay: a new membrane for the fast prediction of passive human skin permeability. *J Med Chem.* 2006;49:3948–54.
10. Hatanaka T, Inuma M, Sugibayashi K, Morimoto Y. Prediction of skin permeability of drugs. I. Comparison with artificial membrane. *Chem Pharm Bull.* 1990;38:3452–9.
11. Geinoz S, Rey S, Boss G, Bunge AL, Guy RH, Carrupt PA, *et al*. Quantitative structure: permeation relationships for solute transport across silicone membranes. *Pharm Res.* 2002;19:1622–9.

12. Hasegawa T, Kim S, Tsuchida M, Isshiki Y, Kondo S, Sugibayashi K. Decrease in skin permeation and antibacterial effect of parabens by a polymeric additive, poly(2-methacryloyloxyethyl phosphorylcholine -cobutylmetacrylate). *Chem Pharm Bull.* 2005;53:271-6.
13. Herkenne C, Naik A, Kalia YN, Hadgraft J, Guy RH. Ibuprofen transport into and through skin from topical formulations: *In vitro-in vivo* comparison. *J Invest Dermatol.* 2007;127:135-42.
14. Hada N, Hasegawa T, Takahashi H, Ishibashi T, Sugibayashi K. Cultured skin loaded with tetracycline HCl and chloramphenicol as dermal delivery system: mathematical evaluation of the cultured skin containing antibiotics. *J Control Release.* 2005;108:341-50.
15. Scheuplein RJ, Blank IH. Mechanism of percutaneous absorption. IV. Penetration of nonelectrolytes (alcohols) from aqueous solutions and from pure liquids. *J Invest Dermatol.* 1973;60:286-96.
16. Scheuplein RJ. Mechanism of percutaneous absorption: transient diffusion and the relative importance of various routes of skin penetration. *J Invest Dermatol.* 1967;48:79-88.
17. Watanabe T, Hasegawa T, Takahashi H, Ishibashi T, Sugibayashi K. Utility of three-dimensional cultured human skin model as a tool to evaluate skin permeation drugs. *Altern Animal Test Experiment.* 2001;8:1-14.
18. Ghanem AH, Mahmoud H, Higuchi WI, Liu P. The effects of ethanol on the transport of lipophilic and polar permeants across hairless mouse skin: methods/validation of a novel approach. *Int J Pharm.* 1992;78:137-56.
19. Sugibayashi K, Hosoya K, Morimoto Y, Higuchi WI. Effect of the absorption enhancer, Azone, on the transport of 5-fluorouracil across hairless rat skin. *J Pharm Pharmacol.* 1985;37:578-80.
20. Pedersen S, Marra F, Nicoli S, Santi P. *In vitro* skin permeation and retention of parabens from cosmetic formulations. *Int J Cosmetic Sci.* 2007;29:361-7.
21. Moser K, Kriwet K, Naik A, Kalia YN, Guy RH. Passive skin penetration enhancement and its quantification *in vitro*. *Eur J Pharm Biopharm.* 2001;52:103-12.
22. Okumura M, Sugibayashi K, Ogawa K, Morimoto Y. Skin permeability of water-soluble drugs. *Chem Pharm Bull.* 1986;37:1404-6.
23. Washitake M, Yajima T, Anmo T, Arita T, Hori R. Studies on percutaneous absorption of drugs. 3. Percutaneous absorption of drugs through damaged skin. *Chem Pharm Bull.* 1973;21:2444-51.
24. Sugibayashi K, Hayashi T, Morimoto Y. Simultaneous transport and metabolism of ethyl nicotinate in hairless rat skin after its topical application: the effect of enzyme distribution in skin. *J Control Release.* 1999;62:201-8.
25. Wilson BW, Walker CR. Regulation of newly synthesized acetylcholinesterase in muscle cultures treated with diisopropyl-fluorophosphate. *Proc Natl Acad Sci USA.* 1974;71:3194-8.
26. Sugibayashi K, Hayashi T, Matsumoto K, Hasegawa T. Utility of a three-dimensional cultured human skin model as a tool to ethyl nicotinate in skin. *Drug Metabol Pharmacokin.* 2004;19:352-62.
27. Nagaosa Y, Tanizaki M. Simultaneous determination of zinc(II) and iron(III) in human serum by liquid chromatography using post-column derivatization with 4-(2-pyridylazo)-resorcinol. *J Liquid Chromat Related Technol.* 1997;20:2357-66.
28. Kawase S, Kanno S, Ukai S. Determination of the herbicides paraquat and diquat in blood and urine by gas chromatography. *J Chromat.* 1984;283:231-40.
29. Izquierdo P, Gómez-Hens A, Pérez-Bendito D. Stopped-flow fluorometric determination of ampicillin in serum. *Fresenius' J Analyt Chem.* 1992;342:606-8.
30. Morimoto Y, Sugibayashi K, Hosoya K, Higuchi WI. Penetration enhancer effect of Azone on the transport of 5-fluorouracil across hairless rat skin. *Int J Pharm.* 1986;32:31-8.
31. Vaughan CD. Solubility effect in product, package, penetration and preservation. *Cosmet Toilet.* 1988;103:47-69.
32. Fedors RF. A method for estimating both the solubility parameters and molar volumes of liquids. *Polym Eng Sci.* 147 (1974).
33. LaPack MA, Tou JC, McGuffin VL, Enke CG. The correlation of membrane permselectivity with Hildebrand solubility parameters. *J Membrane Sci.* 1994;86:263-80.
34. Dias M, Hadgraft J, Lane ME. Influence of membrane-solvent-solute interactions on solute permeation in model membranes. *Int J Pharm.* 2007;336:108-14.

家具及び家電製品からの揮発性有機化合物の放散に関する研究

香川 (田中) 聡子, 神野透人#, 古川容子, 西村哲治

Volatile Organic Compounds (VOCs) Emitted from Furniture and Electrical Appliances

Toshiko Tanaka-Kagawa, Hideto Jinno#, Yoko Furukawa, and Tetsuji Nishimura

Organic chemicals are widely used as ingredients in household products. Therefore, furniture and other household products as well as building products may influence the indoor air quality. This study was performed to estimate quantitatively influence of household products on indoor air quality. Volatile organic compound (VOC) emissions were investigated for 10 products including furniture (chest, desk, dining table, sofa, cupboard) and electrical appliances (refrigerator, electric heater, desktop personal computer, liquid crystal display television and audio) by the large chamber test method (JIS A 1912) under the standard conditions of 28°C, 50% relative humidity and 0.5 times/h ventilation. Emission rate of total VOC (TVOC) from the sofa showed the highest; over 7900 μg toluene-equivalent/unit/h. Relatively high TVOC emissions were observed also from desk and chest. Based on the emission rates, the impacts on the indoor TVOC were estimated by the simple model with a volume of 17.4 m^3 and ventilation frequency of 0.5 times/h. The estimated TVOC increment for the sofa was 911 $\mu\text{g}/\text{m}^3$, accounting for almost 230% of the provisional target value, 400 $\mu\text{g}/\text{m}^3$. The values of estimated increment of toluene emitted from cupboard and styrene emitted from refrigerator were 10% and 16% of guideline values, respectively. These results revealed that VOC emissions from household products may influence significantly indoor air quality.

Keywords: indoor air, emission of volatile organic compounds, household products, large chamber test method

1. はじめに

シックハウス症候群や本態性多種化学物質過敏状態など室内空気の汚染に起因すると考えられる健康被害の増加に伴い、室内環境中の化学物質に対して大きな関心が寄せられている。このような化学物質に関する安全対策としての取り組みとして、化学物質の室内濃度指針値について「シックハウス（室内空気汚染）問題に関する検討会」の中間報告書¹⁾に基づき、これまでにホルムアルデヒド、トルエン及びキシレン等13物質について室内濃度指針値が策定されている。室内における化学物質の主要な発生源の一つである建材に関しては、2003年7月1日に施行された改正建築基準法等²⁾によって低減化

対策が講じられつつある。一方、居住者によって家庭内に持ち込まれる様々な家庭用品にも多種多様な化学物質が使用されており、室内空気の汚染源としての可能性が指摘されているが、それらの製品から放散される化学物質の室内空気への負荷については情報が限られている。本研究では、家庭用品からの化学物質の発生状況を把握し、室内空気中の化学物質に対する家庭用品の寄与を定量的に検討する目的で、大形家具及び家電製品について大形チャンバー法による揮発性有機化合物 (VOC) の放散試験を実施し、室内環境中濃度に対する影響について考察を行った。

2. 実験方法

2.1 試験試料及び放散試験

家具5製品 (タンス, 学習机 (椅子付), テーブル (椅子付), ソファ, 食器棚及びレンジ収納庫), 家電製品5製品 (冷蔵庫, 電気ストーブ, デスクトップ型パーソ

#To whom correspondence should be addressed:

Hideto Jinno; 1-18-1 Kamiyoga, Setagaya-ku, Tokyo 158-8501, Japan; Tel: +81-3-3700-1141 ext.257, Fax +81-3-3707-6950; E-mail:jinno@nihs.go.jp

ナルコンピューター、液晶テレビ及びオーディオ)を試験対象として、大形チャンバー法 (JIS A 1912) に準拠して放散試験を実施した。放散試験には5.5 m³チャンバー (日測エンジニアリング社製) または1 m³チャンバー (エスベック社製) を使用した。液晶テレビ及びオーディオは1 m³チャンバーを、それ以外の試料については5.5 m³チャンバーを用いた。チャンバー内は温度28°C、湿度50%に設定し、換気回数が0.5回になるように純空気を供給した。検体をチャンバー内に設置し24時間後に3層 (Tenax TA/Carbograph 1TD/Carboxen 1000) の吸着管TO-17/2 (Markes) を使用して、50 mL/minの流速で5 L及び2 Lの放散ガスをサンプリングした。家電製品はチャンバー内において稼働時に近い状態に設置して放散試験を実施した。なお、冷蔵庫に関しては通電なし開扉、及び通電あり閉扉の異なる2条件で放散試験を行った。

2.2 加熱脱離GC/MS (TD-GC/MS) による個別VOCs及びTVOCの定量

TD-GC/MSによるVOCsの測定は島津製作所製加熱脱着装置TDTS-2010及びGC/MS-QP-2010を用いて以下に示した条件で行った。

加熱脱着装置付GC/MSの分析条件

加熱脱離 (島津製作所 (株) 製 TDTS-2010)

Desorption : 280°C, 50 mL He/min, 10 min
Cold Trap Temp : -10°C

GC/MS (島津製作所 (株) 製 GC/MS-QP2010)

Column : Rtx-1 (0.32 mm×60 m, 1µm)
Carrier Gas : He, 2.35 ml/min
Column Temp. : 40°C -5°C/min-250°C
Interface Temp. : 250°C
Ion Source Temp. : 200°C
Scan Range : m/z 35-350

測定対象化合物は、平成15年度及び平成16年度に国立医薬品食品衛生研究所において実施した「室内空気中の揮発性有機化合物に関する全国調査」の結果より室内空気中で高頻度に検出される化学物質として選定した70種のVOC³⁾とした。定量は2 ng - 250 ngの範囲で個別に行った。また、*n*-ヘキサンから*n*-ヘキサデカンの間の保持時間に溶出されるトータルイオンクロマトグラムのピーク面積積分値からtotal VOC (TVOC) 量を算出してトルエン換算値として示した³⁾。デコンボリューション解析にはAnalyzerPro (SpectralWorks) を使用し、

シミラリティー検索のためのマススペクトルライブラリーとして、NIST 05及びFFNSC GC/MS香料ライブラリー (島津製作所) を用いた。

2.3 解析

放散ガス中の各VOC濃度から次式により各検体について単位試料当たりの放散速度 (µg/(m²·h)) を算出した。なお、放散速度の算出においては原則的に試料空気として5L捕集した吸着管を用いて分析した結果を採用することとした。分析結果が定量範囲 (250 ng) を超えた場合には、試料空気として2L捕集した吸着管を用いて分析した結果を採用した。

〈計算式〉 $EF = C \times n \times V$

EF : 単位個数当たりの放散速度 (µg/unit/h)
C : チャンバー内のVOCの濃度 (µg/m³)
= 測定対象物質の質量 (ng) / 空気捕集量 (l)
n : 換気回数 (回/h)
V : チャンバーの容積 (m³)

個別定量物質及びTVOCの定量下限 (2 ng) から放散速度の定量下限を以下のように設定した。

◇5.5 m³チャンバーを用いた放散試験 (Sample ID#: 1-9) における放散速度の定量下限
試料空気として5L捕集した場合 : 1.1 µg/unit/h
試料空気として2L捕集した場合 : 2.8 µg/unit/h

◇1 m³チャンバーを用いた放散試験 (Sample ID#: 10, 11) における放散速度の定量下限
試料空気として5L捕集した場合 : 0.2 µg/unit/h
試料空気として2L捕集した場合 : 0.5 µg/unit/h

また、次式により気中濃度増分値 ΔC (µg/m³) を算出した。

$$\Delta C = \frac{EF \times UR}{nR \times VR}$$

ΔC : 気中濃度増分値 (µg/m³)
UR : 個数 (unit)
EF : 単位個数当たりの放散速度 (µg/unit/h)
nR : 室内空気モデル内の換気回数 (0.5回/h)
VR : 室内空気モデル内の体積 (17.4 m³)

3. 結果及び考察

家具5製品及び家電製品5製品を対象として大形チャンバー法により各製品から放散されるVOCを測定しTVOC量として算出した結果をTable 1に示した。TVOCとして総体的に評価した結果では、家具からのTVOC放散量が高い傾向が認められた。中でもソファからの放散量が7924 μg トルエン相当量/unit/hと最も高く、学習机・椅子やタンスでも比較的高いTVOCの放散が認められた(それぞれ4825, 3401 μg トルエン相当量/unit/h)。ソファについては、デコンポリューション解析の結果からロンギフォレン, カリオフィレン, テルピネオール等の木材由来のテルペン類が主要なTVOC構成成分であると考えられるが、BHTが比較的高い放散量(377 μg トルエン相当量/unit/h)を示したことが特筆される点である。BHTに関しては、学習机・椅子(109 μg トルエン相当量/unit/h)やテーブル・椅子(298 μg トルエン相当量/unit/h)からも検出されており、多種、多様な家庭用品からの放散によって室内環境への負荷が累積的に増加する可能性についても考慮する必要がある。

個別定量対象物質の測定結果をTable 2に示した。尚、表中の試料ID番号に対応する試料名についてはTable 1と同様である。

(家具)

タンス (ID# 1) : 酢酸メチル (129.8 μg /unit/h), 酢酸ブチル (83.9 μg /unit/h), アセトン (71.6 μg /unit/h), 1-ブタノール (49.8 μg /unit/h) 及び*n*-テトラデカン (48.6 μg /unit/h) が比較的高い放散速度の高い化合物として検出された。これらの他に、デコンポリューション解析により酢酸 (553 μg トルエン相当量/unit/h), メトキシプロ

パノールアセテート (182 μg トルエン相当量/unit/h), δ -カジネン (112 μg トルエン相当量/unit/h), α -アモルフェン (86 μg トルエン相当量/unit/h), α -テルピネオール (64 μg トルエン相当量/unit/h) 及び1,2,3,5-テトラメチルベンゼン (61 μg トルエン相当量/unit/h) が暫定的に同定された。

学習机・椅子 (ID# 2) : *m*-, *p*-キシレン (236.4 μg /unit/h), 1-ブタノール (162.8 μg /unit/h), 2-プロパノール (129.5 μg /unit/h), 酢酸ブチル (82.4 μg /unit/h), *o*-キシレン (49.8 μg /unit/h) が比較的高い放散速度の高い化合物として検出された。これらの他に、デコンポリューション解析により酢酸 (1026 μg トルエン相当量/unit/h), α -グルジュネン (507 μg トルエン相当量/unit/h), メトキシプロパノールアセテート (302 μg トルエン相当量/unit/h), 2-ブトキシエタノール (218 μg トルエン相当量/unit/h), 3-エトキシプロピオン酸エチル (175 μg トルエン相当量/unit/h), δ -エレメン (143 μg トルエン相当量/unit/h), BHT (ブチルヒドロキシルトルエン) (109 μg トルエン相当量/unit/h) が暫定的に同定された。

テーブル・椅子 (ID# 3) : *m*-, *p*-キシレン (550.3 μg /unit/h), *o*-キシレン (115.8 μg /unit/h), 酢酸ブチル (108.2 μg /unit/h), エチルベンゼン (48.2 μg /unit/h) が比較的高い放散速度の高い化合物として検出された。これらの他に、デコンポリューション解析によりBHT (298 μg トルエン相当量/unit/h), 酢酸 (218 μg トルエン相当量/unit/h), 2-ブトキシエタノール (78 μg トルエン相当量/unit/h) が暫定的に同定された。

Table 1 Emission rate of TVOC from furniture and electrical appliances

試料ID	試料名	TVOC放散速度 (μg Toluene/unit/h)	気中濃度増分子測値 (μg Toluene/ m^3)	TVOC暫定目標値*に 対する比率 (%)	Deconvolution法で 暫定的に同定された化 合物の比率 (%)
ID# 1	タンス	3,401	391	98	67
ID# 2	学習机・椅子	4,825	555	139	80
ID# 3	テーブル・椅子	1,600	184	46	95
ID# 4	ソファ	7,924	911	228	54
ID# 5	食器棚及びレンジ収納庫	2,875	330	83	69
ID# 6	冷蔵庫 (通電なし閉扉)	2,127	245	61	100
ID# 7	冷蔵庫 (通電あり閉扉)	713	82	20	105
ID# 8	電気ストーブ	164	19	5	90
ID# 9	デスクトップ型PC	1,524	175	44	34
ID# 10	液晶テレビ	1,440	166	41	104
ID# 11	オーディオ	417	48	12	100

* 400 $\mu\text{g}/\text{m}^3$

Table 2 Emission rate of VOCs from furniture and electrical appliances

	Emission Rate ($\mu\text{g}/\text{unit}/\text{h}$)										
	ID# 1	ID# 2	ID# 3	ID# 4	ID# 5	ID# 6	ID# 7	ID# 8	ID# 9	ID# 10	ID# 11
Acetone	71.6	42.0	12.3	41.9	91.4		12.8	16.3	173.7	10.1	54.6
2-Propanol		129.5									8.8
Methyl acetate	129.8	38.4	10.8	9.2	34.1						3.2
Dichloromethane										20.5	2.1
2-Methylpentane	15.0										
Methylethylketone	2.3	10.9	11.1	8.9	20.8	25.2	3.7		4.9	2.6	30.1
3-Methylpentane											
Ethyl acetate										13.1	
<i>n</i> -Hexane						54.4					
Chloroform											
2,4-Dimethylpentane/Methylcyclopentane											
Methylcyclopentane/2,4-Dimethylpentane						5.2					
1,1,1-Trichloroethane											
1-Butanol	49.8	162.8	16.6		8.2	26.2	8.4	18.3	32.0	OR	6.6
Benzene											1.0
1-Methoxy-2-propanol	26.7		7.4								2.4
Carbon tetrachloride											
Cyclohexane											
2-Methylhexane											
3-Methylhexane											
Trichloroethylene											
2,2,4-Trimethylpentane											
<i>n</i> -Heptane											
Methylisobutylketone	6.4	16.2	30.4								
Methylcyclohexane											
Isobutyl acetate		1.3									
Toluene*	19.2	15.5	29.2	26.8	230.4	8.6	2.3		12.3	OR	30.3
1,4-dimethylcyclohexane											
Butyl acetate	83.9	82.4	108.2	2.4	24.7						
<i>n</i> -Octane											
Tetrachloroethylene											
Ethylbenzene*	1.8	41.5	48.2	4.9	3.7	55.7	9.1		39.7	5.1	2.5
<i>m</i> -, <i>p</i> -Xylene*	17.2	236.4	550.3	22.2		67.2	12.7	8.9	100.5	33.4	14.3
2-Methyloctane						32.8	4.8				
3-Methyloctane											
Styrene*	2.3	4.1	3.9	13.8	12.1	307.6	146.4		64.4	3.2	89.5
<i>o</i> -Xylene*		49.3	115.8	3.0	4.3	3.4			19.4	3.0	2.5
<i>n</i> -Nonane											
Isopropylbenzene			2.9						1.1		
3,5-Dimethyloctane											
α -Pinene	2.2			7.4		5.2	3.1		7.4		
<i>n</i> -Propylbenzene			7.8								
(+/-)-Camphene											
Phenol	3.0	28.6	43.5	7.2	4.3	13.8	9.1	15.3	57.6	OR	47.5
1,3,5-Trimethylbenzene			8.8	1.3							
2-Methylnonane											
alpha-Methylstyrene										2.4	
2-Ethyltoluene		1.6	7.0								
β -Pinene											
2-Pentylfuran			1.7		2.8						
1,2,4-Trimethylbenzene		11.2	32.8	6.2	2.2						1.1
<i>n</i> -Decane											7.5
1,4-Dichlorobenzene	8.0	20.4	6.5	51.9	6.2						
3-Carene											
1,2,3-Trimethylbenzene		2.8		2.7	1.2						
Limonene											
1-Methyl-3-propylbenzene											
<i>n</i> -Butylbenzene			1.1								
<i>n</i> -Undecane	2.2								1.6		5.5
1,2,4,5-Tetramethylbenzene	32.1	5.2		1.8	3.4						
1,3,5-Trichlorobenzene			1.5								
Camphor				8.8							
Naphthalene	11.8	12.7	2.7	32.1	3.1				2.3		0.8
<i>n</i> -Dodecane	16.8		4.8	2.8	2.4	5.5	1.2		10.9		5.9
<i>n</i> -Tridecane	33.2		4.4	10.1	2.5		4.5		6.2		
<i>n</i> -Tetradecane	48.6	11.1	14.8	42.1	2.1	17.4	21.2		29.5	2.7	17.8
<i>n</i> -Pentadecane	41.8	1.5	3.8	60.2	5.2		1.6		10.2		0.5
TXIB											
<i>n</i> -Hexadecane	24.5	4.8	24.5	46.1	5.1	3.2	16.4		19.9		5.6

* : 室内温度指針値が策定されている化学物質

OR : 定量範囲外

空欄 : 定量下限値未満

ソファ (ID# 4): *n*-ペンタデカン (60.2 µg/unit/h), 1,4-ジクロロベンゼン (51.9 µg/unit/h), *n*-ヘキサデカン (46.1 µg/unit/h) が比較的放散速度の高い化合物として検出された。これらの他に、デコンボリユーション解析によりロンギフォレン (1659 µgトルエン相当量/unit/h), カリオフィレン (432 µgトルエン相当量/unit/h), BHT (377 µgトルエン相当量/unit/h), テルピネオール (169 µgトルエン相当量/unit/h), ロンギシクレン (142 µgトルエン相当量/unit/h), α -ロンギピネン (124 µgトルエン相当量/unit/h), カリオフィレン (93 µgトルエン相当量/unit/h), 酢酸 (89), テトラメチルブタンジニトリル (89 µgトルエン相当量/unit/h), (+)-サチベン (65 µgトルエン相当量/unit/h), ジヒドロ- α -テルピネオール (57 µgトルエン相当量/unit/h) が暫定的に同定された。

食器棚 (ID# 5): トルエン (230.4 µg/unit/h), アセトン (91.4 µg/unit/h) が比較的放散速度の高い化合物として検出された。これらの他に、デコンボリユーション解析により酢酸 (988 µgトルエン相当量/unit/h), (+)-ロンギフォレン (87 µgトルエン相当量/unit/h), 2-メチルプロパン酸1-(1,1-ジメチルエチル)-2-メチル-1,3-プロパンジイルエステル (81 µgトルエン相当量/unit/h), ヘキサナール (64 µgトルエン相当量/unit/h), ギ酸 (57 µgトルエン相当量/unit/h) が暫定的に同定された。

〈家電製品〉

冷蔵庫 (通電なし・開扉) (ID# 6): スチレン (307.6 µg/unit/h), *m*-, *p*-キシレン (67.2 µg/unit/h), エチルベンゼン (55.7 µg/unit/h), *n*-ヘキサン (54.4 µg/unit/h) が比較的放散速度の高い化合物として検出された。これらの他に、デコンボリユーション解析により2,7,10-トリメチルドデカン (256 µgトルエン相当量/unit/h), ウンデカン (200 µgトルエン相当量/unit/h), シクロペンタン (110 µgトルエン相当量/unit/h), 4,7-ジメチルウンデカン (110 µgトルエン相当量/unit/h), ヘキサデカン (105 µgトルエン相当量/unit/h), ペンタデカン (85 µgトルエン相当量/unit/h), ウンデカン (60 µgトルエン相当量/unit/h) 及び2,4-ジメチルヘプタン (51 µgトルエン相当量/unit/h) が暫定的に同定された。

冷蔵庫 (通電あり・閉扉) (ID# 7): スチレン (146.4 µg/unit/h) が比較的放散速度の高い化合物として検出された。これらの他に、デコンボリユーション解析によりシクロペンタン (131 µgトルエン相当量/unit/h) が暫定的に同定された。

電気ストーブ (ID# 8): 顕著な放散速度を示す個別定量対象物質は検出されなかった。デコンボリユーション解析により1,3-ジアセチルベンゼン (62 µgトルエン相当量/unit/h) が暫定的に同定された。

デスクトップ型PC (ID# 9): アセトン (173.7 µg/unit/h), *m*-, *p*-キシレン (100.5 µg/unit/h), スチレン (64.4 µg/unit/h), フェノール (57.6 µg/unit/h) が比較的放散速度の高い化合物として検出された。

液晶テレビ (ID# 10): 1-ブタノール, トルエン, フェノールの3物質が極めて高い濃度で検出されたものの、定量範囲の上限 (絶対量として250 ng) を超えたため、正確な定量は困難であった。測定機器の感度を適宜調節した上でTVOCとして再測定した結果、デコンボリユーション解析により酢酸ブチル (515 µgトルエン相当量/unit/h), シクロヘキサノン (386 µgトルエン相当量/unit/h), トルエン (197 µgトルエン相当量/unit/h), 1-ブタノール (110 µgトルエン相当量/unit/h), フェノール (83 µgトルエン相当量/unit/h) が暫定的に同定された。

オーディオ (ID# 11): スチレン (89.5 µg/unit/h), アセトン (54.6 µg/unit/h), フェノール (47.5 µg/unit/h) が比較的放散速度の高い化合物として検出された。

測定の結果得られた各VOCの放散速度を基に、デンマーク規格の室内空間モデル (容積17.4 m³, 換気率0.5回/hの室内を想定したモデル) を用いて室内空間への負荷濃度 (気中濃度増分値) を予測した。その結果をTable 3に示した。

個別定量対象の70化合物では食器棚から放散されるトルエンが室内濃度指針値 (260 µg/m³) の約10%, テーブル・椅子から放散されるキシレン (*o*-キシレン, *m*-キシレン及び*p*-キシレンの総和として) が室内濃度指針値 (870 µg/m³) の約9%, 開扉状態の冷蔵庫から放散されるスチレンが室内濃度指針値 (220 µg/m³) の約16%に相当する濃度の負荷を引き起こす可能性があることが示唆された。冷蔵庫について実際の使用時を想定した状態 (閉扉通電状態) で試験した結果ではスチレンの負荷濃度は開扉状態の47%まで減少するものの、室内濃度指針値に対する占有率は依然として約8%であり、室内空気中のスチレンに関して冷蔵庫が重要な汚染源となる可能性があると考えられる。さらに、冷蔵庫の断熱材に関して興味深い点は、デコンボリユーション解析によって、開扉無通電、閉扉通電何れの状態の冷蔵庫からもシクロペンタンの放散が確認されたことである (放散速度はそ

Table 3 The increment of VOC concentrations in indoor environment estimated by its emission rate

	Estimated VOC Increment ($\mu\text{g}/\text{m}^3$)										
	ID# 1	ID# 2	ID# 3	ID# 4	ID# 5	ID# 6	ID# 7	ID# 8	ID# 9	ID# 10	ID# 11
Acetone	8.2	4.8	1.4	4.8	10.5		1.5	1.9	20.0	1.2	6.3
2-Propanol		14.9									1.0
Methyl acetate	14.9	4.4	1.2	1.1	3.9						0.4
Dichloromethane										2.4	0.2
2-Methylpentane	1.7										
Methylethylketone	0.3	1.3	1.3	1.0	2.4	2.9	0.4		0.6	0.3	3.5
3-Methylpentane											
Ethyl acetate										1.5	
<i>n</i> -Hexane						6.3					
Chloroform											
2,4-Dimethylpentane/Methylcyclopentane											
Methylcyclopentane/2,4-Dimethylpentane						0.6					
1,1,1-Trichloroethane											
1-Butanol	5.7	18.7	1.9		0.9	3.0	1.0	2.1	3.7	OR	0.8
Benzene											0.1
1-Methoxy-2-propanol	3.1		0.8								0.3
Carbon tetrachloride											
Cyclohexane											
2-Methylhexane											
3-Methylhexane											
Trichloroethylene											
2,2,4-Trimethylpentane											
<i>n</i> -Heptane											
Methylisobutylketone	0.7	1.9	3.5								
Methylcyclohexane											
Isobutyl acetate		0.1									
Toluene* ($260\mu\text{g}/\text{m}^3$)	2.2	1.8	3.4	3.1	26.5	1.0	0.3		1.4	OR	3.5
1,4-dimethylcyclohexane											
Butyl acetate	9.6	9.5	12.4	0.3	2.8						
<i>n</i> -Octane											
Tetrachloroethylene											
Ethylbenzene* ($3800\mu\text{g}/\text{m}^3$)	0.2	4.8	5.5	0.6	0.4	6.4	1.1		4.6	0.6	0.3
<i>m</i> -, <i>p</i> -Xylene* ($870\mu\text{g}/\text{m}^3$)	2.0	27.2	63.3	2.6		7.7	1.5	1.0	11.6	3.8	1.6
2-Methyloctane						3.8	0.6				
3-Methyloctane											
Styrene* ($220\mu\text{g}/\text{m}^3$)	0.3	0.5	0.4	1.6	1.4	35.4	16.8		7.4	0.4	10.3
<i>o</i> -Xylene* ($870\mu\text{g}/\text{m}^3$)		5.7	13.3	0.3	0.5	0.4			2.2	0.3	0.3
<i>n</i> -Nonane											
Isopropylbenzene			0.3						0.1		
3,5-Dimethyloctane											
α -Pinene	0.3			0.9		0.6	0.4		0.9		
<i>n</i> -Propylbenzene			0.9								
(+/-)-Camphene											
Phenol	0.3	3.3	5.0	0.8	0.5	1.6	1.0	1.8	6.6	OR	5.5
1,3,5-Trimethylbenzene			1.0	0.2							
2-Methylnonane											
alpha-Methylstyrene										0.3	
2-Ethyltoluene		0.2	0.8								
β -Pinene											
2-Pentylfuran			0.2		0.3						
1,2,4-Trimethylbenzene		1.3	3.8	0.7	0.2						0.1
<i>n</i> -Decane											0.9
1,4-Dichlorobenzene	0.9	2.3	0.7	6.0	0.7						
3-Carene											
1,2,3-Trimethylbenzene		0.3		0.3	0.1						
Limonene											
1-Methyl-3-propylbenzene											
<i>n</i> -Butylbenzene			0.1								
<i>n</i> -Undecane	0.3								0.2		0.6
1,2,4,5-Tetramethylbenzene	3.7	0.6		0.2	0.4						
1,3,5-Trichlorobenzene			0.2								
Camphor				1.0							
Naphthalene	1.4	1.5	0.3	3.7	0.4				0.3		0.1
<i>n</i> -Dodecane	1.9		0.6	0.3	0.3	0.6	0.1		1.3		0.7
<i>n</i> -Tridecane	3.8		0.5	1.2	0.3		0.5		0.7		
<i>n</i> -Tetradecane	5.6	1.3	1.7	4.8	0.2	2.0	2.4		3.4	0.3	2.0
<i>n</i> -Pentadecane	4.8	0.2	0.4	6.9	0.6		0.2	1.2		0.1	
TXIB											
<i>n</i> -Hexadecane	2.8	0.5	2.8	5.3	0.6	0.4	1.9		2.3		0.6

* : 室内温度指針値が策定されている化学物質 (括弧内の数字 : 室内濃度指針値, ¹⁾ : Xyleneとして)

OR : 定量範囲外

空欄 : 定量下限値未満

れぞれ110 μg トルエン相当量/unit/h, 131 μg トルエン相当量/unit/h). これは冷蔵庫に使用される断熱材のノンフロン化に伴ってシクロペンタンが代替発泡剤として用いられつつあることを反映した結果であると考えられ、建築用断熱材に使用されるノンフロン代替発泡剤の動向も踏まえて室内環境への負荷を注意深く見守る必要がある。

本調査で個別に定量した化合物のうち上述したトルエン、キシレン及びスチレン以外に室内濃度指針値が策定されている物質として、エチルベンゼンがあげられるが、本調査においては特に高濃度に検出された試料は認められず、最も高い放散量を示した試料（冷蔵庫：通電なし開扉）でも室内濃度指針値（3800 $\mu\text{g}/\text{m}^3$ ）の1%以下であった。

デスクトップ型PCからのVOCの放散に関しては、(社)電子情報技術産業協会 (JEITA) による自主的なガイドラインとして、トルエン、キシレン、1,4ジクロロベンゼン、エチルベンゼン、スチレンに指針値が設定されている（それぞれ130, 435, 120, 1900, 110 $\mu\text{g}/\text{unit}/\text{h}$ ）。本調査で採用した放散試験の諸条件はJEITAの試験法と若干異なっているものの、上記の5物質についてはJEITA指針値を満たす結果が得られた。ただし、TVOCとして評価した場合、その放散速度は1524 $\mu\text{g}/\text{unit}/\text{h}$ と高い値を示しており、1440 $\mu\text{g}/\text{unit}/\text{h}$ の液晶テレビとともに室内環境における重要なTVOC負荷源であると言えよう。さらに、デスクトップ型PCに関してはデコンポリューション解析で同定された化合物の比率が全ての検体の中で最も低い値となっており、シリコン化合物と考えられる未同定物質の放散が認められる点も今後の検討課題と言えるかもしれない。

4. まとめ

本調査では家庭用品による室内空気への化学物質の負荷を明らかにする目的で家具5品目、電化製品5品目、計10品目の大型家庭用品について放散試験を実施し、個別定量対象の70化合物及びTVOCについて測定を行った。その結果、個別定量対象の化合物では食器棚から放散されるトルエンが室内濃度指針値（260 $\mu\text{g}/\text{m}^3$ ）の約10%、開扉状態の冷蔵庫から放散されるスチレンが室内濃度指針値（220 $\mu\text{g}/\text{m}^3$ ）の約16%に相当する濃度の負荷を引き起こす可能性があることが示唆された。

また、各製品からの揮発性有機化合物の放散をTVOCとして総体的に評価した結果では、家具からのTVOC放散量が高い傾向が認められた。中でもソファからの放散量が最も高く、TVOC暫定目標値の2倍以上の負荷を引き起こす可能性が示された。学習机・椅子やタンスか

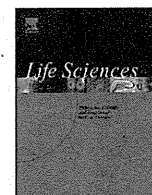
らも高いTVOCの放散が認められ、それぞれの気中濃度増分予測値はTVOC暫定目標値の138%、98%であった。デスクトップ型PC及び液晶テレビからも比較的高いTVOCの放散が認められ予測される気中濃度増分値はそれぞれ44%、41%であり、ともに室内環境における重要なTVOC負荷源となり得ることが示された。

謝辞

本研究を実施するに当たりご助言賜りました厚生労働省医薬食品局審査管理部化学物質安全対策室・柴辻正喜氏並びに古田光子氏に深謝いたします。

参考文献

- 1) Safety Control of Sick House Syndrome (Indoor Air Pollution) inistry of Health, Labour and Welfare (<http://www.mhlw.go.jp/new-info/kobetu/seikatu/kagaku/>)
- 2) Shick house countermeasure based on Standards Law : Ministry of Land, Infrastructure, Transport and Tourism (<http://www.mlit.go.jp/jutakukentiku/build/sickhouse.html>)
- 3) Hideto Jinno et al., :Study on Evaluating method of Volatile Organic Compounds (VOCs) Emitted from Household Products. Health and Labor Science Research Grants, Research Project on Risk of Chemicals, Research Report (2006).



Functional characterization of human and cynomolgus monkey UDP-glucuronosyltransferase 1A1 enzymes

Nobumitsu Hanioka^{a,*}, Natsuko Tanabe^a, Hideto Jinno^b, Toshiko Tanaka-Kagawa^b, Kenjiro Nagaoka^a, Shinsaku Naito^c, Akiko Koeda^d, Shizuo Narimatsu^a

^a Graduate School of Medicine, Dentistry and Pharmaceutical Sciences, Okayama University, 1-1-1 Tsushima-naka, Kita-ku, Okayama 700-8530, Japan

^b Division of Environmental Chemistry, National Institute of Health Sciences, 1-18-1 Kamiyoga, Setagaya-ku, Tokyo 158-8501, Japan

^c Research and Development Center, Otsuka Pharmaceutical Factory, Inc., 115 Kuguhara, Tateiwa, Muya-cho, Naruto, Tokushima 772-8601, Japan

^d Department of Metabolism and Analytical Research, Ina Research Inc., 2148-188 Nishiminowa, Ina, Nagano 399-4501, Japan

ARTICLE INFO

Article history:

Received 17 March 2010

Accepted 30 June 2010

Keywords:

UDP-glucuronosyltransferase (UGT)
UGT1A1

7-Hydroxy-4-trifluoromethylcoumarin (7-HFC)

Estradiol at 3-hydroxy position (E-3OH)

7-Ethyl-10-hydroxycamptothecin (SN-38)

Human

Cynomolgus monkey

ABSTRACT

Aims: UDP-glucuronosyltransferase 1A1 (UGT1A1) plays important roles in the glucuronidation of various drugs and endogenous substances. Cynomolgus monkeys are regarded as experimental animals closer to humans in studies on safety evaluation and biotransformation for drug development. In this study, the similarities and differences in the enzymatic properties of UGT1A1 between humans and cynomolgus monkeys were precisely identified.

Main methods: Human and cynomolgus monkey UGT1A1s (humUGT1A1 and monUGT1A1, respectively) were cloned, and the corresponding proteins were heterologously expressed in insect cells. The enzymatic properties of UGT1A1 proteins were characterized by kinetic analysis of 7-hydroxy-4-trifluoromethylcoumarin (7-HFC), estradiol at 3-hydroxy position (E-3OH) and 7-ethyl-10-hydroxycamptothecin (SN-38) glucuronidation.

Key findings: There were no significant differences in the levels of kinetic parameters for 7-HFC, E-3OH and SN-38 glucuronidation between humans and cynomolgus monkeys in both enzyme sources of liver microsomes and recombinant UGT1A1s. 7-HFC and E-3OH glucuronidation by human liver microsomes exhibited biphasic and sigmoidal kinetics, respectively, whereas the kinetics by cynomolgus monkey liver microsomes fitted the typical Michaelis–Menten model. SN-38 glucuronidation by human and cynomolgus monkey liver microsomes exhibited autoactivation kinetics. In recombinant UGT1A1 enzymes expressed in insect cells, the kinetics of 7-HFC, E-3OH and SN-38 glucuronidation fitted the substrate inhibition (7-HFC glucuronidation) or Hill equation (E-3OH and SN-38 glucuronidation), and each glucuronidation showed the same kinetic profile between humans and cynomolgus monkeys.

Significance: These findings suggest that the enzymatic properties of human and cynomolgus monkey UGT1A1 enzymes are very similar.

© 2010 Elsevier Inc. All rights reserved.

Introduction

UDP-glucuronosyltransferases (UGTs) are membrane-bound enzymes that are localized inside the endoplasmic reticulum, and catalyze the conjugation of various endogenous substances (e.g. bile acids, bilirubin and steroids) and xenobiotics (e.g. drugs and environmental toxicants) to glucuronide (Ritter 2000; Tukey and Strassburg 2000). Consistent with their broad substrate profiles, UGTs are known to exist as a superfamily of independently regulated enzymes. The UGT superfamily is divided into many subfamilies on the basis of evolutionary divergence. Among the human UGT superfamily, two families (UGT1 and UGT2) and three subfamilies (UGT1A, UGT2A and

UGT2B) are predominantly involved in glucuronidation (Mackenzie et al. 1997, 2005). The *UGT1A* gene is localized on chromosome 2q37 and encodes proteins with unique amino-terminal domains and identical carboxyl-terminal domains, which are formed from the alternate mRNA splicing of unique first exons with common exons 2–5. In contrast, *UGT2A* and *UGT2B* genes are clustered on chromosome 4q13 and individual UGT proteins are encoded by unique genes with six exons (Mackenzie et al. 1997, 2003, 2005; Guillemette 2003). Each UGT exhibits unique substrate and tissue specificities (Ritter 2000; Tukey and Strassburg 2000; Kiang et al. 2005).

UGT1A1 is expressed in the liver, bile duct, stomach and colon, and plays an important role in the detoxification of neurotoxic bilirubin by conjugating it with glucuronic acid for excretion in bile (Iyanagi et al. 1998; Tukey and Strassburg 2000). A reduced level of UGT1A1 activity has been reported to be associated with unconjugated hyperbilirubinemia (Crigler–Najjar syndrome and Gilbert's syndrome) (Mackenzie et al.

* Corresponding author. Tel./fax: +81 86 251 7943.

E-mail address: hanioka@pharm.okayama-u.ac.jp (N. Hanioka).

1997; Tukey and Strassburg 2000; Guillemette 2003). UGT1A1 also catalyzes the glucuronidation of 7-ethyl-10-hydroxycamptothecin (SN-38), the active metabolite of an anticancer drug, irinotecan (CPT-11, 7-ethyl-10-[4-(1-piperidino)-1-piperidino]carbonyloxy camptothecin), to form inactive SN-38 glucuronide (Iyer et al. 1998; Hanioka et al. 2001). Furthermore, wide interindividual variability in SN-38 glucuronide formation in hepatic tissues is known and has been shown to correlate with a *UGT1A1* genetic factor (Iyer et al. 1998, 1999; Guillemette 2003); therefore, *UGT1A1* polymorphisms have been regarded to be one of the most important factors for irinotecan efficacy and toxicity (Ando and Hasegawa 2005; Hasegawa et al. 2006; Ando et al. 2007).

Many UGT enzymes have been suggested to be expressed in hepatic and/or extrahepatic tissues of mammals, including humans, monkeys, rats and mice (Mackenzie et al. 1997, 2005; Tukey and Strassburg 2000), and the cDNAs of several isoforms have been cloned (<http://som.flinders.edu.au/FUSA/ClinPharm/UGT/udgpa.html>). In general, nonhuman primates, such as rhesus monkeys (*Macaca mulatta*) and cynomolgus monkeys (*Macaca fascicularis*), are regarded as experimental animals closer to humans in studies on safety evaluation and biotransformation for drug development; therefore, examination of the functional characterization of monkey UGT enzymes is an important aspect of drug metabolism research. Vallée et al. (2001) cloned cynomolgus monkey UGT1A1 (monUGT1A1) cDNA encoding an ortholog of human UGT1A1 (humUGT1A1), and qualitatively determined the catalytic activities toward estrogens of recombinant monUGT1A1 expressed in HEK293 cells; however, detailed kinetic analyses of xenobiotic glucuronidation by the recombinant enzyme were not included. Furthermore, there has been no report on the quantitative function characterization of human and cynomolgus monkey UGT1A1s using both enzyme sources of liver microsomes and recombinant enzymes.

The purpose of this study was to precisely identify the similarities and differences in the enzymatic properties of UGT1A1 between humans and cynomolgus monkeys. To achieve this, human and cynomolgus monkey UGT1A1 enzymes were heterologously expressed in insect cells, and the enzymatic properties were subsequently examined by kinetic analyses for the glucuronidation of 7-hydroxy-4-trifluoromethylcoumarin (7-HFC), estradiol at 3-hydroxy position (E-3OH), and SN-38.

Materials and methods

Materials

Three individual human liver microsomes (two men, 41 and 55 years old; one woman, 56 years old) and rabbit anti-human UGT1A1 antibody were purchased from BD Biosciences (San Jose, CA, USA). Three male cynomolgus monkey livers (4 years old, 2.7–2.9 kg) were supplied by Ina Research Inc. (Nagano, Japan). Cynomolgus monkey liver microsomes were prepared as described previously (Hanioka et al. 2006). The use of human and cynomolgus monkey livers for this study was approved by the ethics review boards of Okayama University. *HindIII* was purchased from Takara Bio (Shiga, Japan); pGEM-T vector was from Promega (Madison, WI, USA); pFastBac1 vector, Bac-to-Bac Baculovirus Expression System and *Spodoptera frugiperda* (Sf9) cells were from Invitrogen (Carlsbad, CA, USA); 7-HFC, 7-HFC glucuronide and E-3OH glucuronide were from Sigma-Aldrich (St. Louis, MO, USA); and estradiol was from Wako Pure Chemical Industries (Osaka, Japan). SN-38 and SN-38 glucuronide were supplied by Yakult Honsha (Tokyo, Japan). UDP-glucuronic acid was purchased from Nacalai Tesque (Kyoto, Japan); peroxidase-conjugated goat anti-rabbit immunoglobulin was from Zymed Laboratories (South San Francisco, CA, USA); and Enhanced ChemiLuminescence Plus was from GE Healthcare Bio-Sciences (Little Chalfont, UK). All other chemicals and reagents used were of the highest quality commercially available.

Expression of recombinant UGT1A1 enzymes

humUGT1A1 cDNA was amplified by polymerase chain reaction (PCR) from humUGT1A1 cDNA cloned into pcDNA3.1 vector (Jinno et al. 2003) as a template using the forward primer 5'-AAGCTTAAAAAATGGCTGTGGAGTCCCA-3' and the reverse primer 5'-AAGCTTCAATGGGTCTTGGATTGTGGG-3'. The *HindIII* sites (underlined letters) were introduced at the 5'-end of the start codon and the 3'-end of the stop codon to facilitate subcloning into pFastBac1 vector. The cDNA encoding monUGT1A1 was amplified by nested PCR from cynomolgus monkey liver single-strand cDNA, prepared as described previously (Hanioka et al. 2006). The nucleotide sequences of the forward and reverse primers used were 5'-ATGGCTGTGGAGTCCCAAGG-CAGACATC-3' and 5'-CTCGAGTCTCAATGGGTCTTGGATTGTGG-3' for first PCR, and AAGCTTAAAAAATGGCTGTGGAGTCCCA-3' and 5'-AAGCTTCAATGGGTCTTGGATTGTGGG-3' for second PCR. The PCR products of hum UGT1A1 and monUGT1A1 cDNAs were directly introduced into pGEM-T vector using TA cloning, and sequenced in both forward and reverse directions to confirm that there were no PCR errors. The cDNA fragments corresponding of humUGT1A1 and monUGT1A1 were cut from the pGEM-T plasmids with *HindIII*, and were subsequently subcloned into pFastBac1 vector digested with *HindIII*. The expression plasmids were sequenced to verify the correct orientation with respect to the promoter (polyhedrin promoter) for pFastBac1 vector.

Recombinant baculovirus carrying humUGT1A1 or monUGT1A1 cDNA was generated using the Bac-to-Bac Baculovirus Expression System according to the manufacturer's protocol. For protein expression, Sf9 cells (2.0×10^8 cells/flask) were infected with recombinant baculoviruses at a multiplicity of infection of 1.0. The cells were harvested at 72 h post-infection, and suspended in 50 mM Tris-HCl buffer (pH 7.4) containing 0.25 M sucrose, 0.1 mM dithiothreitol, 0.1 mM EDTA and 0.5 mM phenylmethylsulfonyl fluoride. The cell suspensions were sonicated 20 times with 10-s bursts, following by centrifugation at 105,000 g for 60 min to obtain membrane fractions. The resulting pellets were resuspended in 50 mM Tris-HCl (pH 7.4) containing 20% glycerol and stored at -80°C until use. Total protein concentrations were determined by the method of Lowry et al. (1951) using bovine serum albumin as a standard.

Recombinant UGT1A1s (1.0 μg protein) as well as liver microsomes (20 μg protein) of humans and cynomolgus monkeys were separated by 10% sodium dodecyl sulfate-polyacrylamide gel electrophoresis (Laemmli 1970) and electrotransferred to a polyvinylidene fluoride sheet, as described by Towbin et al. (1979). The sheet was incubated with rabbit anti-human UGT1A1 antibody (diluted at 1:5000) as the primary antibody and then with peroxidase-conjugated goat anti-rabbit immunoglobulin (diluted at 1:5000) as the secondary antibody. Immunoreactive proteins were visualized with chemifluorescence (Enhanced ChemiLuminescence Plus), and band densities were relatively determined with ImageJ v1.42 (National Institute of Health Sciences, Bethesda, MD, USA).

Assay for UGT1A1-dependent enzymatic activities

Glucuronidation activities toward 7-HFC, E-3OH and SN-38 were determined by high-performance liquid chromatography as described previously with some modifications (Hanioka et al. 2001; Alkharfy and Frye 2002; Brill et al. 2006). The incubation mixture contained 7-HFC (1.0–200 μM), estradiol (0.5–100 μM) or SN-38 (0.5–100 μM) as a substrate, liver microsomes or recombinant UGT1A1s, 10 mM MgCl_2 and 5 mM UDP-glucuronic acid in a final volume of 500 μL of 50 mM Tris-HCl buffer (pH 7.4). The protein concentrations of liver microsomes and recombinant UGT1A1s were 10 and 50 $\mu\text{g}/\text{mL}$ for 7-HFC and SN-38 glucuronidation assays, and 50 and 50 $\mu\text{g}/\text{mL}$ for the E-3OH glucuronidation assay. The substrates were dissolved in

methanol/dimethyl sulfoxide (50:50, v/v) for 7-HFC and estradiol, and dimethyl sulfoxide/0.05 N NaOH (50:50, v/v) for SN-38. The final concentration of the organic solvent (methanol and/or dimethyl sulfoxide) in the incubation mixture was 1% (v/v). After preincubation for 2 min at 37 °C, the reaction was initiated by adding UDP-glucuronic acid. Incubation was performed for 10 min (7-HFC and SN-38 glucuronidation assay) or 20 min (E-3OH glucuronidation assay) at 37 °C and terminated by adding 50 µL of 10% phosphoric acid and vortexing. The samples were centrifuged at 12,000 g for 10 min at 4 °C. The supernatant was filtered with a polytetrafluoroethylene membrane filter (0.45 µm pore size; Millipore, Bedford, MA, USA), and a 20 µL portion of the filtrate was subjected to high-performance liquid chromatography.

The high-performance liquid chromatographic system consisted of an L-2130 pump (Hitachi, Tokyo, Japan), an L-2300 column oven (Hitachi), an L-2480 fluorescence detector (Hitachi), and a Rheodyne type 7725i (Hitachi) injector equipped with an Inertsil ODS-SP (4.6 mm i.d. × 150 mm; GL Sciences, Tokyo, Japan) for 7-HFC and SN-38 glucuronidation assays or an Inertsil Ph (4.6 mm i. d. × 150 mm; GL Sciences) for the E-3OH glucuronidation assay. The column was maintained at 40 °C. Data acquisition was accomplished using D-2000 Elite v1.1 software. 7-HFC glucuronide was eluted isocratically with 20 mM KH₂PO₄ (pH 3.5)/acetonitrile/methanol (62:26:12, v/v/v) at a flow rate of 1.0 mL/min. Fluorometric detection was performed with excitation at 328 nm and emission at 410 nm. Retention times of 7-HFC glucuronide and 7-HFC were 3.5 and 18.9 min, respectively. The limit of detection for 7-HFC glucuronide was 5.0 pmol/assay. E-3OH glucuronide was eluted isocratically with 20 mM KH₂PO₄ (pH 3.0)/acetonitrile (70:30, v/v) at a flow rate of 1.0 mL/min. Fluorometric detection was performed with excitation at 210 nm and emission at 300 nm. Retention times of E-3OH glucuronide and estradiol were 3.8 and 13.0 min, respectively. The limit of detection for E-3OH glucuronide was 10 pmol/assay. SN-38 glucuronide was eluted isocratically with 20 mM KH₂PO₄ containing 2 mM sodium 1-octanesulphonate (pH 2.5)/acetonitrile/methanol (72:22:6, v/v/v) at a flow rate of 1.0 mL/min. Fluorometric detection was performed

with excitation at 370 nm and emission at 425 nm. Retention times of SN-38 glucuronide and SN-38 were 3.3 and 16.3 min, respectively. The limit of detection for SN-38 glucuronide was 0.2 pmol/assay. Standard curve samples spiked with 7-HFC glucuronide (10–5000 pmol/mL), E-3OH glucuronide (20–1000 pmol/mL) or SN-38 glucuronide (1.0–50 pmol/mL) for both assays were prepared in the same manner as incubation samples. Intra-day (n = 5) and inter-day (n = 5) precision did not exceed 10% in any of the assays.

Data analysis

Kinetic constants (K_m or S_{50} , V_{max} , and K_{si}) and the Hill coefficient (n) for 7-HFC, E-3OH and SN-38 glucuronidation were calculated by constructing velocity versus substrate concentration ([S]-[V]) and Eadie-Hofstee ([V/S]-[V]) plots using SigmaPlot v8.02 software (Systat Software, San Jose, CA, USA). The kinetic profile was estimated by comparison of r^2 among Michaelis-Menten, substrate inhibition, isoenzyme and Hill equations. In vitro clearance values were CL_{int} (V_{max}/K_m) or CL_{max} ($V_{max}/S_{50} * (n-1)/(n(n-1)^{1/n})$). All values are expressed as the mean ± S.D. of three donors/animals or three separate experiments derived from independent preparations. Statistical comparisons were made with an unpaired two-tailed Student's *t*-test, and differences were considered significant when the *p* value was <0.05.

Results

Sequence analysis of humUGT1A1 and monUGT1A

Sequence analysis determined that humUGT1A1 and monUGT1A1 cDNA has an open reading frame of 1602 bp, encoding the respective proteins of 533 amino acids. The nucleotide sequence of humUGT1A1 was identical to that of cDNA characterized previously (GenBank accession no. NM_000463). In monUGT1A1, one silent mutation (1401A>G, Arg467Arg) was found compared with the cDNA cloned by Vallée et al. (2001) (GenBank accession no. AF104339). Fig. 1 shows the alignment of the deduced amino acid sequences between

humUGT1A1	1	MAVESQGGRRPLVLGLLLCVLPVVS	HAGKILLIPVDGSHWLSMLGAI	QQLQQRGHEIVVL	60
monUGT1A1	1	MAVESQGRHPLVLGLLLCVLPVLC	HAGKMLLIPVDGSHWLSMLGTT	QQLQQRGHEIVVL	60
		*****	*****	*****	*****
humUGT1A1	61	APDASLYIRDGAFYTLKTYPPVF	QREDVKESFVSLGHNVFENDS	SFLQRVIKTYKKIKKDS	120
monUGT1A1	61	APDASLYIREGAFYTLKTYPPVF	QREDVKESFVSLGHNVFENDS	SFLRRVIKTYKKIKKDS	120
		*****	*****	*****	*****
humUGT1A1	121	AMLLSGCSHLLHNKELMASLAESS	FDVMLTDPFLPCSPIVAQYLS	LPVFFLHALPCSLE	180
monUGT1A1	121	AMLLSGCSHLLHNKELMASLAESS	FDVMLTDPFLPCGPPIVAQYLS	LPVFFLNALPCSLE	180
		*****	*****	*****	*****
humUGT1A1	181	FEATQCPNPFYSVPRPLSSHSDH	MTFLQRVKNMLIAFSQNF	LCDVVVSPYATLASEFLQR	240
monUGT1A1	181	SEATQCPNPFYSVPRPLSAHSDH	MTFLQRVKNMLIAFSQNF	LCDVVVSPYATLASEFLQR	240
		*****	*****	*****	*****
humUGT1A1	241	EVTVQDLLSSASVWVLRSDFKD	YPRPIMPNMVFGGINCLHQ	NPLSQEFEAYINASGEH	300
monUGT1A1	241	EVTVQNLLSSASVWVLRSDFKD	YPRPIMPNMAFIGGINCLHQ	SPLSQEFEAYINASGEH	300
		*****	*****	*****	*****
humUGT1A1	301	GIVVFSLGSVMVSEIPEKKAMA	IADALGKIPQTVLWRYTG	TRPSNLANNITLVKWL	PQNDL 360
monUGT1A1	301	GIVVFSLGSMAEIEPEKKAMA	IADALGKIPQTVLWRYTG	TPPSNLANNITLVKWL	PQNDL 360
		*****	*****	*****	*****
humUGT1A1	361	LGHMPTRAFITHAGSHGVYESI	CNGVPMVMPLFGDQMDNA	KRMETRGAGVTLNVLE	MTS 420
monUGT1A1	361	LGHMPTRAFITHAGSHGIYEG	ICNGVPMVMPLFGDQMDNA	KRMETRGAGVTLNVLE	MTS 420
		*****	*****	*****	*****
humUGT1A1	421	EDLENALKAVINDKSYKENIM	RLSSSLHKDRPVEPLD	LAVFWVEFVMRHKGAP	HLRPA 480
monUGT1A1	421	EDLENALKAVINDKSYKENIM	HLSSSLHKDRPVEPLD	LAVFWVEFVMRHKGAP	HLRPA 480
		*****	*****	*****	*****
humUGT1A1	481	LWTYQYHSLDVI	GFLLAIVLTVAFITFK	CWAYGRKCLGKKG	RVKKAHKS 533
monUGT1A1	481	LWTYQYHSLDVI	GFLLAIVLTVAFIAPK	CWAYGRKCFGKKG	RVKKAHKS 533
		*****	*****	*****	*****

Fig. 1. Deduced amino acid sequence alignment of humUGT1A1 and monUGT1A1. Asterisks indicate the same amino acid residues between humUGT1A1 and monUGT1A1.

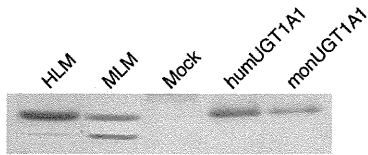


Fig. 2. Immunoblotting of liver microsomes and insect cell membranes expressing UGT1A1s of humans and cynomolgus monkeys. Representative results of pooled samples from three independent preparations are expressed. Protein levels applied were 1.0 $\mu\text{g}/\text{lane}$ for recombinant UGT1A1s and 20 $\mu\text{g}/\text{lane}$ liver microsomes. HLM, human liver microsomes; MLM, cynomolgus monkey liver microsomes.

humUGT1A1 and monUGT1A1. The homology between humUGT1A1 and monUGT1A1 was 95% at the amino acid level.

Expression of humUGT1A1 and monUGT1A1 enzymes

Human and cynomolgus monkey UGT1A1 enzymes were expressed separately in insect cells. Fig. 2 shows immunoblotting for liver microsomes and insect cell membranes expressing UGT1A1s of humans and cynomolgus monkeys using anti-human UGT1A1 antibody. All enzyme sources except the negative control (mock) yielded immunodetectable UGT1A1 protein; however, the staining band intensities of cynomolgus monkey liver microsomes and insect cells expressing monUGT1A1 were weak compared with those from enzyme sources in humans. The relative levels were human liver microsomes (100) and cynomolgus monkey liver microsomes (51), and humUGT1A1 (100) and monUGT1A1 (42), where human values were normalized to 100.

Enzymatic properties of humUGT1A1 and monUGT1A1 enzymes

Kinetic analyses of 7-HFC, E-3OH and SN-38 glucuronidation by recombinant humUGT1A1 and monUGT1A1 as well as by human and cynomolgus monkey liver microsomes were then performed. No activity in insect cell membranes of the negative control (mock) was

Table 1

Kinetic parameters for 7-HFC glucuronidation by liver microsomes and recombinant UGT1A1s of humans and cynomolgus monkeys.

	K_m (μM)	V_{\max} (nmol/min/mg protein)	CL_{int} ($\mu\text{L}/\text{min}/\text{mg}$ protein)	K_{si} (μM)
HLM				
High-affinity phase	2.58 ± 1.66	2.94 ± 1.43	1240 ± 250	
Low-affinity phase	30.1 ± 3.9	14.4 ± 6.8	479 ± 208	
MLM	16.1 ± 1.9	25.9 ± 2.9	1610 ± 100	
humUGT1A1	198 ± 47	7.10 ± 2.07	35.2 ± 2.9	99.6 ± 19.9
monUGT1A1	151 ± 74	3.90 ± 2.31	24.8 ± 3.0	161 ± 76

Each value represents the mean \pm SD of three separate experiments derived from independent preparations. HLM, human liver microsomes; MLM, cynomolgus monkey liver microsomes.

detected with any substrate (data not shown). The plots ($[S]-[V]$ and $[V/S]-[V]$ plots) and parameters of kinetics are shown in Fig. 3 and Table 1 for 7-HFC glucuronidation, Fig. 4 and Table 2 for E-3OH glucuronidation, and Fig. 5 and Table 3 for SN-38 glucuronidation.

7-HFC glucuronidation by human liver microsomes exhibited a biphasic kinetic profile, and K_m values for high- and low-affinity phases were 2.6 and 30 μM , respectively. V_{\max} and CL_{int} values were 2.9 nmol/min/mg protein and 1200 $\mu\text{L}/\text{min}/\text{mg}$ protein for the high-affinity phase, and 14 nmol/min/mg protein and 480 $\mu\text{L}/\text{min}/\text{mg}$ protein for the low-affinity phase, respectively. In cynomolgus monkey liver microsomes, the kinetics of 7-HFC glucuronidation was monophasic with a K_m value of 16 μM . V_{\max} and CL_{int} values were 1.8- and 1.3-fold higher than those of low- and high-affinity phases in human liver microsomes, respectively. 7-HFC glucuronidation by recombinant human and cynomolgus monkey UGT1A1s exhibited substrate inhibition kinetics with K_{si} values of 100 μM for humUGT1A1 and 160 μM for monUGT1A1. K_m , V_{\max} and CL_{int} values

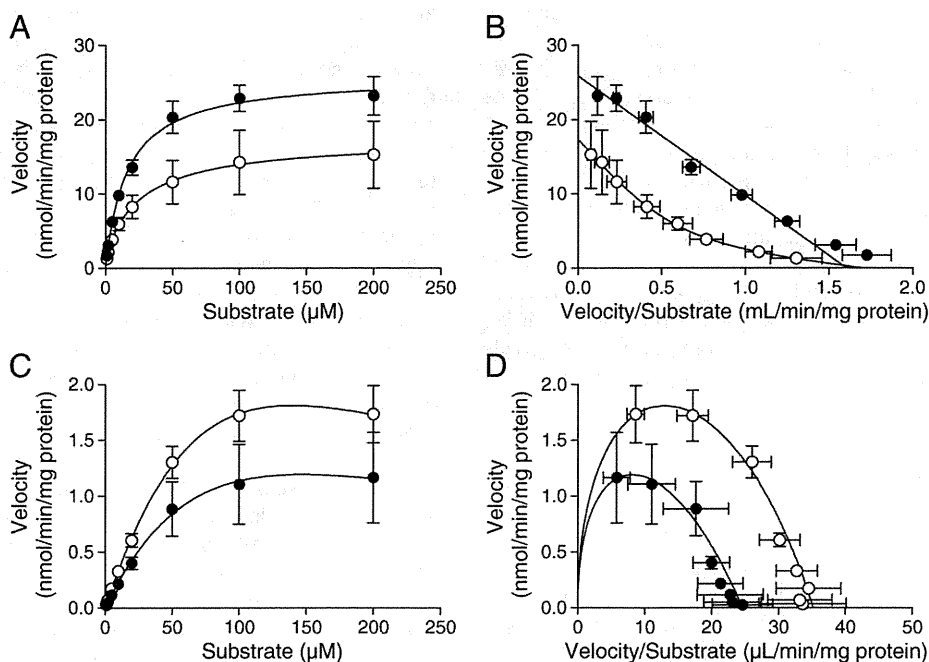


Fig. 3. Kinetics for 7-HFC glucuronidation by liver microsomes and insect cell membranes expressing UGT1A1s of humans and cynomolgus monkeys. Substrate concentrations were 1.0–200 μM . Each point represents the mean \pm SD of three separate experiments derived from independent preparations. (A) $[S]-[V]$ plots for liver microsomes; (B) $[V/S]-[V]$ plots for liver microsomes; (C) $[S]-[V]$ plots for insect cell membranes expressing UGT1A1s; (D) $[V/S]-[V]$ plots for insect cell membranes expressing UGT1A1s. \circ , human liver microsomes or humUGT1A1; \bullet , cynomolgus monkey liver microsomes or monUGT1A1.

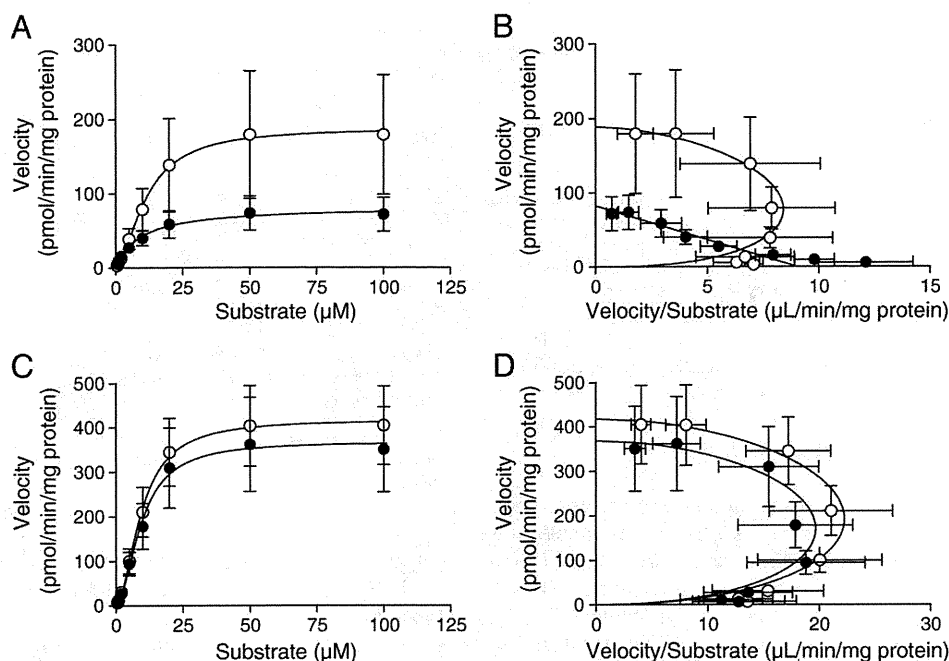


Fig. 4. Kinetics for E-3OH glucuronidation by liver microsomes and insect cell membranes expressing UGT1A1s of humans and cynomolgus monkeys. Substrate concentrations were 0.5–100 μM . Each point represents the mean \pm SD of three separate experiments derived from independent preparations. (A) [S]–[V] plots for liver microsomes; (B) [V/S]–[V] plots for liver microsomes; (C) [S]–[V] plots for insect cell membranes expressing UGT1A1s; (D) [V/S]–[V] plots for insect cell membranes expressing UGT1A1s. \circ , human liver microsomes or humUGT1A1; \bullet , cynomolgus monkey liver microsomes or monUGT1A1.

of humUGT1A1 were 200 μM , 7.1 nmol/min/mg protein and 35 μL /min/mg protein, respectively. The levels of monUGT1A1 were not significantly different from those of humUGT1A1.

E-3OH glucuronidation by human liver microsomes followed sigmoidal kinetics with n of 1.7, which manifests as a curvilinear [V/S]–[V] plot. S_{50} , V_{max} and CL_{max} values were 11 μM , 190 pmol/min/mg protein and 11 μL /min/mg protein, respectively. In contrast, the kinetics of E-3OH glucuronidation by cynomolgus monkey liver microsomes was fitted to the monophasic Michaelis–Menten model. K_m and CL_{int} values were comparable to those of S_{50} and CL_{max} for human liver microsomes, respectively, whereas the V_{max} value was 44% that of human liver microsomes. E-3OH by recombinant human and cynomolgus monkey UGT1A1s exhibited sigmoidal kinetics with n of 1.9 for both humUGT1A1 and monUGT1A1. S_{50} , V_{max} and CL_{max} values of humUGT1A1 were 9.5 μM , 420 pmol/min/mg protein and 30 μL /min/mg protein, respectively. The levels of monUGT1A1 were comparable to those of humUGT1A1.

SN-38 glucuronidation by liver microsomes and recombinant UGT1A1s of humans and cynomolgus monkeys exhibited sigmoidal kinetics. The n of liver microsomes and recombinant UGT1A1 of humans were 1.4 and 1.9, respectively. S_{50} , V_{max} and CL_{max} of humans were 7.4 μM , 49 pmol/min/mg protein and 4.2 μL /min/mg protein for liver microsomes, and 6.8 μM , 130 pmol/min/mg protein and 13 μL /min/mg protein for recombinant UGT1A1, respectively. These param-

eter levels for sigmoidal kinetics of cynomolgus monkeys were comparable to those of humans in both liver microsomes and recombinant UGT1A1.

Discussion

UGT1A1, a member of the UGT superfamily, plays an important role in the glucuronidation of various endogenous substances and medicines (Ritter 2000; Tukey and Strassburg 2000; Kiang et al. 2005). UGT1A1 activity and expression have also been shown to be influenced by genetic, physiological and environmental factors (Tukey and Strassburg 2000; Mackenzie et al. 2003). Although monkeys, including cynomolgus monkeys, are commonly used as an animal model for the development of medicines, and particularly for the characterization of pharmacokinetics and toxicological properties of novel molecules, little is known about the enzymatic properties of novel UGT enzymes. The functional evaluation of human and cynomolgus monkey UGT1A1 enzymes should provide important information for the prediction and extrapolation of drug metabolism. Enzymatic activities in insect cells expressing human and cynomolgus monkey UGT1A1s were therefore investigated by kinetic analysis. To this end, we used 7-HFC, E-3OH and SN-38 glucuronidation as the probes for UGT1A1.

The expression of UGT1A1 proteins was confirmed by Western blot analysis. Anti-human UGT1A1 antibody recognized the corresponding UGT1A1s in livers microsomes and insect cell membranes expressing UGT1A1s of humans and cynomolgus monkeys, and the intensities of staining bands for liver microsomes and recombinant UGT1A1 of cynomolgus monkeys were about 50–40% those of humans. This phenomenon is thought to occur because the cross-reactivity with UGT1A1 proteins of the antibody used in this study differed between human and cynomolgus monkey UGT1A1s.

The active site of UGT enzymes is on the luminal side of the endoplasmic reticulum, resulting in an in vitro latency (Radomska-Pandya et al. 1999; Tukey and Strassburg 2000). To overcome this phenomenon in vitro, alamethicin (pore-forming agent) is commonly used as an alternative to detergents (Fisher et al. 2000a, 2001).

Table 2

Kinetic parameters for E-3OH glucuronidation by liver microsomes and recombinant UGT1A1s of humans and cynomolgus monkeys.

	K_m or S_{50} (μM)	V_{max} (pmol/min/mg protein)	n	CL_{int} or CL_{max} (μL /min/mg protein)
HLM	11.3 \pm 0.7	189 \pm 86	1.66 \pm 0.15	10.5 \pm 4.7
MLM	8.79 \pm 2.04	82.4 \pm 28.9		9.23 \pm 1.07
humUGT1A1	9.47 \pm 0.39	418 \pm 93	1.86 \pm 0.06	29.6 \pm 7.0
monUGT1A1	9.42 \pm 0.15	368 \pm 103	1.85 \pm 0.05	26.2 \pm 8.0

Each value represents the mean \pm SD of three separate experiments derived from independent preparations. HLM, human liver microsomes; MLM, cynomolgus monkey liver microsomes.